X-690-75-55
PREPRINT

ANGULAR DISTRIBUTIONS, KINETIC ENERGY DISTRIBUTIONS, AND EXCITATION FUNCTIONS OF FAST METASTABLE OXYGEN FRAGMENTS FOLLOWING ELECTRON IMPACT OF CO_2

M. MISAKIAN
M. J. MUMMA
J. F. FARIS

MARCH 1975

GODDARD SPACE FLIGHT CENTER
GREENBELT, MARYLAND

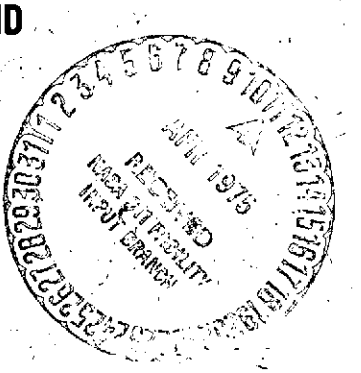

For information concerning availability
of this document contact:

Technical Information Division, Code 250
Goddard Space Flight Center
Greenbelt, Maryland 20771

(Telephone 301-982-4488)

ANGULAR DISTRIBUTIONS, KINETIC ENERGY DISTRIBUTIONS, AND EXCITATION FUNCTIONS OF FAST METASTABLE OXYGEN FRAGMENTS FOLLOWING ELECTRON IMPACT OF CO_2

by

M. Misakian*
Institute for Fluid Dynamics
and Applied Mathematics
University of Maryland
College Park, Maryland 20771

and

M. J. Mumma**
J. F. Faris
Laboratory for Extraterrestiral Physics
NASA/Goddard Space Flight Center
Greenbelt, Maryland 20771

ABSTRACT

Dissociative excitation of CO_2 by electron impact has been studied using the methods of translational spectrosocpy and an angular distribution analysis. Earlier time-of-flight studies revealed two overlapping spectra, the slower of which has been attributed to metastable $CO(a^3\pi)$ fragments. The fast peak is the focus of the present study. Threshold energy, angular distribution and improved time-of-flight measurements indicate that the fast peak actually consists of five overlapping features. The slowest of the five features (1) is found to consist of metastable $O(\overline{^5S})$ produced by predissociation of a Σ_u^+ Sigma u + state of CO_2 into $O(\overline{^5S}) + CO(\overline{a^3\pi})$. Oxygen Rydberg fragments originating directly from a different Σ_u^+ state are believed to make up the next fastest feature (2). Sigma u + Mechanisms for producing the three remaining features are discussed.

* Present Address: AIKEN ELEC/AERO GEO ASTRO, 7411 50th Avenue, College Park, Maryland 20740.
** Author to whom requests for reprints should be sent.

DISSOCIATIVE EXCITATION OF CO_2 BY ELECTRON IMPACT

I. INTRODUCTION

In recent years, the experimental technique of translational spectroscopy has been demonstrated to be quite useful in the study of molecular dissociative excitation processes.[1-5] Typically a molecule is excited by photon or electron impact to a repulsive or predissociating excited state and time-of-flight (TOF) distributions of fragments in long lived excited states (metastable or high-lying Rydberg) are measured. The photo-dissociative TOF work has been limited to processes with vertical excitation energies of $\lesssim$ 5 eV. The electron impact studies have mainly dealt with super-excited molecular states having energies in the range of 10 - 50 eV. In the latter case excitation functions for production of the time resolved fragments allow one to determine, for diatomic molecules, the asymptotic energy (AE) of the relevant excited state potential curve and, in favorable cases, a portion of the potential curve can be constructed. Polyatomic molecules can be similarly examined, but interpretation of the results becomes more complicated because the excess excitation energy above the asymptotic energy[6] of a potential surface need not appear only as translational energy shared by the dissociated fragments. When angular distributions of time resolved fragments are also measured, Dunn's[7] rules can be useful in classifying the symmetry of the excited molecular states. In addition to characterizing the dissociation mechanism, translational spectroscopy can provide knowledge of the released kinetic and electronic energies of the fragment and such information can be of value in understanding the chemistry, thermal properties, excitation processes and composition of upper planetary atmospheres.

Recently, TOF measurements of dissociative excitation of CO_2 by electron impact have revealed that the metastable fragments fall into two well defined energy distributions.[1b,4c] The slower of the two features has been examined in some detail[1b] and attributed to $CO(a^3\pi)$ fragments, but the mechanisms for production of the fast feature (believed to be metastable oxygen) have not been sufficiently explored. In the present study we have focussed our efforts on the fast peak using the methods of translational spectroscopy as well as an angular distribution analysis. It will be seen that the fast peak actually consists of at least five overlapping features and possible mechanisms for their production will be discussed.

II. FRAGMENTATION PROCESSES

Production of metastable oxygen fragments from CO_2 can take place in a number of ways. Direct dissociation may occur by excitation from the ground $X^1\Sigma_g^+$ electronic state potential surface to the repulsive region of an electronically excited surface as shown schematically in Fig. 1(a) for the case of two fragment dissociation. According to the Franck-Condon principle and Born-Oppenheimer approximation, excitation can be thought of as a "verticle leap" within the Franck Condon region to a point Y. A semi-classical description of the molecule's motion as dissociation progresses from Y is given by a surface trajectory of a "mass point", the dynamics of which are governed by the shape of the potential surface. Dissociation need not occur immediately with "one swing" across the surface (as shown) and out one of the potential "valleys", but may be delayed as the mass point first goes through a complicated Lissajous motion over the

potential well.[8] An oscillatory trajectory in the potential valley indicates the vibrational motion of the CO fragment. The highest point of a given trajectory on the valley wall indicates the ro-vibrational energy. While the total excess energy after excitation is equal to the height of Y above the valley floor, only energy exceeding the ro-vibrational energy of the CO fragment is available as translational energy to be partitioned among the O and CO fragments (see Fig. 1(a)). A review and discussion of several models for energy partitioning has recently been given by Wilson and co-workers[3a,9] and will not be presented here. The total released kinetic energy, E_T, is related to the measured oxygen fragment kinetic energy (E_o) (from energy and momentum conservation) by

$$E_T = \frac{M_{CO_2}}{M_{CO}} E_o, \tag{1}$$

where M_{CO_2} and M_{CO} are the masses of CO_2 and CO.

An important consideration when interpreting the measured laboratory fragment energies is the influence of the parent molecule's thermal motion. If a fragment acquires center of mass energy $E_F (E_F \gg kT)$ from the kinetics of the dissociation process and if the molecules in the target gas have a Maxwellian velocity distribution characterized by the temperature T, then the detected fragment will develop an energy spread given by[10]

$$P(E^{1/2}-E_F^{1/2})\, dE = \left[\frac{1}{4\pi\beta kTE_o}\right]^{1/2} \exp\left[-\frac{1}{\beta kT}(E^{1/2}-E_F^{1/2})^2\right] dE. \tag{2}$$

Here $P(E^{1/2}-E_F^{1/2})$ is the fraction of the dissociated fragments having a lab energy between E and E+dE and β is the ratio of detected fragment and parent molecule masses.

Alternatively, the fragmentation may occur through a predissociation[11] process in which excitation to a bound surface (AC'A) is followed by dissociation via a mixing with a nearby surface (AD) or surface crossing (CC'C) as shown schematically in Fig. 1(b). Extension of fragmentation times can again occur because many oscillations in the bound state are expected prior to mixing.

Yet other modes of dissociation include excitation to a saddle point overlooking two potential valleys yielding CO+O and excitation to a purely repulsive surface after which the molecule undergoes total fragmentation. In the latter case no unique determination of the total released kinetic energy can be made.

III. ANGULAR DISTRIBUTION OF FRAGMENTS

Because direct dissociation typically occurs in a time which is short compared to the period of molecular rotation[12], the fragment trajectories will indicate to a good approximation the molecular spatial orientation when excited. Dunn[7] has shown that at threshold, the matrix element behavior for a given electronic transition can depend markedly on the molecular orientation with respect to the electron beam and that in general, anisotropies are to be expected in the observed fragment angular distributions. A portion of Dunn's transition matrix element table is shown in Fig. 2 with qualitative angular distributions for parallel and perpendicular transitions. While this early treatment of the problem was for diatomic molecules, the extension to polyatomic systems is straightforward.[13] In the present study, however, the qualitative predictions of Fig. 2 are applicable because of the linear conformation of CO_2 in the ground state.

More detailed accounts describing possible anisotropies for specific transitions have been given since the work of Dunn. The "practical approximations" developed by Zare and Herschbach[12] for electron energies well above threshold,

$$I(\theta) = A[\cos^2\theta'\cos^2\theta+(1/2)\sin^2\theta'\sin^2\theta] \tag{3}$$

for $\Delta\Lambda = 0$ ($\Sigma \rightarrow \Sigma$, $\pi \rightarrow \pi$, etc.) and

$$I(\theta) = A'[2\cos^2\theta'\sin^2\theta+\sin^2\theta'(1+\cos^2\theta)] \tag{4}$$

for $\Delta\Lambda \neq 0$ ($\Sigma \rightarrow \pi$, $\pi \rightarrow \Delta$, etc.)

have proved to be useful in describing measured angular distributions of H^+ ions[14] and H(2s) neutral fragments[2] from H_2. In Eqs. 3 and 4, Λ is the component of electronic orbital angular momentum along the internuclear axis, θ' is the most probable angle between the momentum transfer vector and electron beam direction; θ is the angle between the electron beam direction and the line along which fragments are observed; A and A' depend on electron energy (but not θ).

Most recently Van Brunt[15] has considered the effect of higher order multipole correction terms to the dipole approximation used to arrive at Eqs. 3 and 4. The influence of the higher order terms on fragment angular distributions can be significant particularly near threshold and when there is large momentum transfer; deviations from the predictions of Eqs. 3 and 4 then become quite pronounced.[16]

Finally we note that fragment angular distributions originating from a predissociation process, or one in which direct dissociation is delayed by complicated Lissajous motion of the mass point, retain

a degree of anisotropy, the extent being determined by the excited molecular state lifetime.[15,17]

IV. APPARATUS

The present experiment was carried out in a vacuum system with a base pressure of approximately 2×10^{-7} torr. A schematic view of the electron gun-detector system is shown in Fig. 3. An approximately monoenergetic ($\sim$ 0.4 eV spread FWHM), pulsed, electrostatically focussed electron beam traversed a scattering cell ($\sim$ 1.6 cm radius) filled with CO_2 gas. Research grade (99.999%) CO_2 gas was purchased from Air Reduction, Inc (AIRCO) and was used directly without further purification. The electron gun was of the Pierce type (ARIS, Model 1000) and the "on pulse" was applied to the Pierce element which was negatively biased. Entrance and exit apertures (two millimeters diameter) to the gas cell provided additional collimation for the electron beam; the electron current to the exit aperture was kept to a few percent of the collector current during angular distribution measurements. The electron gun voltage scale was calibrated by measuring the threshold voltage for producing triplet metastable helium, $He(2^3S)$, and comparing it with the known value of 19.82 eV. A mixture of helium and CO_2 gas was used for this purpose. An MKS Baratron was used to measure the cell pressure which was typically 5×10^{-4} torr. The partial pressure of CO_2 outside the cell was approximately 3.5×10^{-6} torr. A plot of metastable particle counts versus cell pressure was linear to 5.5×10^{-4} torr indicating that collisional quenching within the cell was not significant. Inelastic electron collisions with the gas produced metastable oxygen and CO fragments which then passed through a collimating slit system and were

detected with a brass metal surface (biased 3 volts negative wrt ground) located 12.8 cm away in the field of view of a continuous electron multiplier ("Channeltron", Electro-Optics Division, Bendix Co.). The Channeltron cone was operated at ground potential.

The metastable $O(^1S, 2\ eV)$ and $O(^1D, 4.2\ eV)$ fragments were not detected because of insufficient energy to produce Auger electrons at the metal surface detector. Only metastable particles of ~ 6 eV or more, namely $O(^5S, 9.14\ eV)$, $CO(a^3\pi, 6\ eV)$, possibly higher lying Rydbergs and photons ($\lambda \lesssim 1800\text{Å}$) could be detected. Ions and scattered electrons were removed by electrostatic deflection plates. The angular intensity distribution was measured by rotating the electron gun-collision cell-electron collector assembly with respect to the detector. The angle θ could be varied from 45 to 135 degrees with respect to the electron beam direction. The field of view was < 2 degrees and θ could be set to within 0.1 degree.

The electronics for obtaining time-of-flight (TOF) spectra are shown schematically in Fig. 4. Typically the electron beam was pulsed on for one microsecond every 400 microseconds. Simultaneously with the onset of the pulse, the Davidson digital TOF unit was triggered. Pulses initiated by metastable fragment arrivals at the metal surface detector were amplified, shaped and then fed as events to the TOF unit. The time elapsed between the trigger pulse and each subsequent event pulse (during the next 400 μseconds) was converted to an address location and stored in a buffer stack memory. A count was later stored at each address location in a GEOS (Canberra) 7001 multichannel analyzer (MCA). Thus the system operated as a multiple-stop time-to-channel number convertor. After the build up of sufficient statistics, a permanent graphic record was made on an X-Y recorder, and the data were stored on magnetic tape.

Excitation functions of fragments with times of flight falling in a pre-selected window were measured by sweeping the electron gun energy and gating-on (EG & G, GI200/N gate generator) the discriminator at specified times after the onset of the electron gun pulse. The electron energy was varied with a Kepco programmable power supply which was controlled by a ramp voltage from the MCA operating in the multi-scale mode. Detector pulses by-passed the Davidson TOF unit and were stored directly in the MCA for these measurements. The effect of the electron gun pulse width was to enlarge the time window thus permitting detection of fragments which were faster than the leading edge of the TOF window.[18]

Because the electron current varied with electron energy, a current vs. voltage function was also generated via an electron current (voltage) to frequency conversion and integrated counts proportional to the electron current were stored in the MCA. Fragment excitation functions were then normalized with a channel-by-channel division of fragment signal by the current signal using an on-line computer.

The alignment of the apparatus was first tested by measuring the angular intensity distribution of the OI(^{3}S - ^{3}P) resonance multiplet at 1304 Å. This multiplet was excited by dissociative excitation of O_2 with 100 eV electrons. A CaF_2 window was placed in front of the detector for this measurement in order to restrict the photon bandpass from ~ 1250 Å to ~ 1800 Å. The only strong emission feature which can be excited in this wavelength range by electron impact on O_2 is the OI(1304 Å) multiplet.[19] Theoretically, we expect the photons of the OI(1304 Å) multiplet to have an isotropic angular distribution since

the upper state has L = 0. Our measured angular distribution[20] was isotropic ($45^{o} \leq \theta \leq 135^{o}$) to within experimental error (a few percent) in agreement with theory.

The angular distribution of thermal metastable helium particles (no dissociation) was also measured to provide a further test of the system. Good agreement was found with theoretical predictions.[21]

V. EXPERIMENTAL RESULTS AND DISCUSSION

Introduction

A complete TOF spectrum of metastable fragments from dissociative excitation of CO_2 at 30 eV is shown in Fig. 5 and, aside from a lower detector sensitivity for $CO(a^3\pi)$, agrees essentially with Freund's data measured at this energy.[1b] The slow peak consists of $CO(a^3\pi)$ fragments and the fast peak has been attributed in part to $O(^5S)$ atoms because of its relative insensitivity to the work function of different surfaces.[1b]

With an expanded time scale, Figure 6 shows the evolution of the oxygen TOF peak as a function of electron energy. Several features are readily resolved. Figure 7 presents smooth curves drawn through the data of Fig. 6 with peak heights adjusted to show the relative intensities as a function of electron energy. This normalization was accomplished by measuring the photon TOF intensity as a function of voltage and adjusting the individual fragment TOF spectra accordingly. Near 23 eV, the slowest feature, designated as feature 1, is clearly resolved although it overlaps with the slower $CO(a^3\pi)$ spectrum. Also present is a decaying photon signal which persists long after the electron gun is turned off.[22] Feature 2, the next fastest feature, can be seen as

structure on the leading edge of feature 1 near 30 eV. Both features grow with electron energy up to ~ 50 eV, above which still another feature becomes visible. We turn now to a more detailed account of these fast features and as the data will show, at least five overlapping spectra are actually present.

FEATURE I

A. Threshold Energies and Excitation Functions

Portions of excitation functions for several TOF windows overlapping with feature 1 are shown in Fig. 8. The voltage increments were .272 eV/channel and data runs of over 24 hours were required to obtain the data. The minimum electron energy required to completely dissociate CO_2 and produce a detectable metastable fragment ($O(^5S)$) is 25.7 eV. Since the measured threshold energies are below this value, we conclude that feature 1 results from

$$e + CO_2 \rightarrow CO_2^* \rightarrow CO + O.$$

Because the parent molecule thermal velocities will add to the c.m. velocity of some fragments (Eq. 2), fragments in feature 1 having c.m. TOF's longer than the trailing edge of the time window and with corresponding lower threshold energies will also be detected. Consequently the electron threshold energy will be displaced to a lower value. Assuming (1) a linear dependence on excess incident electron energy and (2) that all the available energy is partitioned into kinetic energy, the excitation function within a few volts of threshold is nearly proportional to

$$\text{Exc. Fcn.} \propto \sum_{E_F=0}^{E_o+\delta E} \left\{ \left[\int_{E_o}^{E_o+\delta E} P(E^{1/2}-E_F^{1/2})dE \right] x(V-V_{T,F}) x Q_F \right\}. \quad (5)$$

$P(E^{1/2}-E_F^{1/2})$ is given by Eq. 2, $V_{T,F}$ is the threshold electron energy for producing fragments of energy E_F and is equal to AE+E_T because of assumption (2), Q_F is its Franck-Condon factor, E_o is the lowest c.m. fragment kinetic energy which can be detected in the absence of thermal effects and δE is the kinetic energy range which can be detected for a given TOF window. Figure 9 shows the relation of several of these parameters on an energy axis. The values of Q_F were estimated from a portion of the energy distribution of feature 1 (see Fig. 12). Electron threshold energies were then calculated assuming asymptotic energies[6] of 20.0, 20.5, 21,0 eV, and are indicated as vertical lines in Fig. 8. Although the scatter in the data near threshold is large, it appears that a possible asymptotic limit exists near 20.5 eV for fragments in feature 1 with kinetic energies over a 1 eV range (~.9 to 1.9 eV). We note that the separated molecule ($CO(a^3\pi)$) - atom ($O(^5S)$) asymptotic energy is 20.6 eV and a possible interpretation of our results is that both fragments are excited to metastable states. We present, following Freund,[1b] Table 1 indicating minimum energies required to produce various CO and O fragments from CO_2. The presence of $CO(a^3\pi)$ fragments is consistent with Freund's excitation function which shows structure at 21.0 $\pm$ .7 eV. With the present model it would appear that at most only the first two or three vibrational levels of $CO(a^3\pi)$ could be excited.

Contributions to feature 1 may also arise through a cascade mechanism. Dissociative excitation can lead to several excited states of CO + $O(^5P)$ after which the $O(^5P)$ state decays to the $O(^5S)$ level. Their higher asymptotic energies (21.7, 22.6, 23.2 and 23.6 eV) would argue against significant contributions initially, however.

A third mechanism which might be responsible for feature 1 is the production and detection of high lying Rydberg oxygen fragments. Freund's earlier work[1b] included measurements of the fast peak (which includes all the present features) using a Rydberg detector as well as an Auger type (metastable) detector. No significant difference was reported between spectra observed using the two different detectors. A Rydberg mechanism as well as the $CO(a^3\pi)$ + $O(^5S)$ scheme described above will be discussed further in section D.

When the TOF window is extended to 40 μseconds (bottom frame, Fig. 8), a weak but sharp feature appears at 18 eV. A TOF of 40 μseconds corresponds to total kinetic energy release of 1.3 eV for an O fragment and 4.1 eV for a CO fragment. Again, assuming that most of the excess electronic energy has been partitioned into kinetic energy, AE's near 16.7 and 13.9 eV are found for O and CO respectively. The nearest $O(^5S)$ + CO AE is about 2 eV displaced from this value while $CO(a^3\pi)$ + $O(^1D)$ lies at 13.5 eV (Table 1). The combination of $CO(X^1\Sigma^+)$ + $O(^5P \rightarrow {}^5S)$, having an AE of 15.7 eV, is yet another possibility. This last mechanism would require a small cross section to explain the weakness of the observed structure and that the CO fragment have rovibrational energy amounting to 1 eV. The $CO(X^1\Sigma^+)$ + $O(^5S)$ combination would require about 2 eV of CO rovibrational energy, but is unlikely because of a parity (+ → -) violation.

Alternatively, the favorable correlation to the 13.5 eV AE for $CO(a^3\pi) + O(^1D)$ and the weakness of the signal because of lower detector efficiency for $CO(a^3\pi)$ is another explanation which cannot be excluded. Indeed, this structure may coincide with one observed by Freund[1b] at 13.2 ± 0.4 eV. The sharp structure is nearly eliminated when a TOF window of 29-38 μseconds is used indicating that the fastest fragments for this transition have kinetic energies near 1.5 eV (TOF = 40 μseconds) if CO.

The excitation function for feature 1 reaches a maximum near 80 eV and then slowly decreases as shown in Fig. 10. The time window used, 27-34 μsec, excluded large contributions from feature 2; an extremely weak $CO(a^3\pi)$ signal was present as an underlying background. We note here that an examination of excitation functions for features 1 and 2 indicates that the most energetic O fragment in feature 1 is near 2.4 eV (24 μsec). The least energetic fragment has been observed to be near 0.5 eV (section C).

B. Angular Distribution

Angular distributions, $I(\theta)$, of feature 1 could not be systematically studied as a function of electron energy because of overlap with features 2 and possibly 3. Figure 11 shows the angular distribution of feature 1 measured near 24 eV. The results were obtained by first measuring the relatively intense photon $I(\theta)$ signal. This was found to be isotropic within experimental error (~2-3%) after multiplying by $\sin\theta$ to correct for changes in interaction volume seen by the detector. Integration times of 700 seconds were sufficient for obtaining these data. Nearly negligible current drifts were corrected for and the pressure remained constant. After the photon distribution was determined, the relatively

weak TOF spectra of feature 1 were measured as a function of angle for much longer integration times and then normalized by dividing the intensity of fragments with TOF's of 30-42 μseconds (0.8 - 1.5 eV) by their respective photon signals. This procedure included a small isotropic contribution from $CO(a^3\pi)$ fragments which have TOF's near 40 μseconds (see Fig. 8). The data in Fig. 11 represent the results of two independent runs. The non-zero minimum at 90^o suggests that feature 1 originates from a parallel transition for which the fragmentation process has been delayed either by predissociation or possibly from a complicated Lissajous trajectory on the excited state potential surface.

C. Energy Distributions

Energy distributions were obtained from TOF spectra and are shown in Fig. 12 as a function of electron energy. The relative contributions from $CO(a^3\pi)$ become quite small at electron impact energies over 100 eV revealing that the least energetic fragments in feature 1 have about 0.5 eV translational energy.

The transformations from TOF (P(t)) to energy (P(E)) distributions were made using the relations

$$P(E)dE = P(t)\ dt \text{ and } E = \frac{mL^2}{2t^2}$$

where m, L and t are fragment mass, path length and TOF respectively. The energy distribution is just

$$P(E) = P(t)\ t^3/ML^2$$

No correction has been made in the energy scale for the 0.8 μseconds wide electron beam pulse width which was used to obtain the spectra.

A finite pulse width introduces more energetic fragments[18] into a given TOF channel and thus makes the average TOF (energy) for that channel somewhat larger. The distortion increases for shorter TOF's (higher energies). In Fig. 12, the spectra are slightly lower at the higher energies because of this effect.

D. Discussion

Assuming the correctness of our AE determination with separated fragments of $CO(a^3\pi) + O(^5S)$, we can eliminate the extended Lissajous trajectory as the cause for delaying dissociation. A parallel transition implies (Fig. 2) that the CO_2 is excited to a Σ_u^+ state. However, the separated fragments of $CO(a^3\pi) + O(^5S)$ cannot arise from a Σ_u^+ state according to the Wigner-Witmer correlation rules. A more likely mechanism is predissociation of the initially excited $CO_2(\Sigma_u^+)$ state by a nearby anti-bonding (along an OC-O bond) $CO_2(\pi_u^+)$ state via a heterogeneous perturbation.[11]

A difficulty which arises with the above model is an apparent violation of the spin selection rule $\Delta S = 0$ in the initial excitation process or possibly during predissociation. This may be seen by "working back" from the separated fragments $CO(a^3\pi) + O(^5S)$. States leading to these fragments which could perturb the initially excited Σ_u^+ state are $CO_2(^3\pi_u, {}^5\pi_u, {}^7\pi_u)$. The predissociation selection rule $\Delta S = 0$ in turn requires the Σ_u^+ state to have multiplicity 3, 5 or 7. Electron exchange during the collision process could yield a needed $^3\Sigma_u^+$ state. However, the excitation functions for such processes usually rise and fall sharply within a few electron volts of threshold in contrast to the cross section for feature 1 (Fig. 10). We note in the earlier study of $CO(a^3\pi)$ fragments by Freund[1b] that similar difficulties appear

to exist. A possible explanation is that feature 1 is a very weak transition (relative to allowed transitions which yield much stronger photon signals) and we are witnessing excitation to a Rydberg $CO_2(^1\Sigma_u^+)$ state which has triplet character because of spin orbit mixing.[23] The weaker triplet component could then mix with a triplet π state to yield $CO(a^3\pi) + O(^5S)$ with the observed excitation function.

Perhaps more serious difficulties are encountered if one attempts to understand feature 1 by assuming that the detected fragments are high lying Rydberg oxygen atoms. Possible asymptotic energies for CO + O (Rydberg) combinations are

$$CO(X^1\Sigma_g^+) + O(R) \quad \ldots\ldots \sim 19.0 \text{ eV} \qquad \text{(a)}$$

$$CO(a^3\pi) + O(R) \quad \ldots\ldots \sim 25.0 \text{ eV} \qquad \text{(b)}$$

Other combinations of CO + O(R) would lie even higher in energy.

Combination (a) must be rejected, however, because the observed threshold energies (Fig. 8) lie between 21 and 24 eV requiring double electron excitation.[24] Combination (b) and others must be rejected because their thresholds lie higher in energy than the observed thresholds.

A theoretical fit (Eq. 3) of the angular distribution in Fig. 10 was not attempted. Jonah's[17] prediction for $I(\theta)$ of a long lived parallel transition is proportional to $1 + \cos^2\theta$ near threshold assuming a $\cos^2\theta$ excitation dependence. Above threshold, $I(\theta)$ should become less anisotropic and in the present case, the contribution of $CO(a^3\pi)$ fragments in the angular distribution data should further reduce the anisotropy. We note that the approximate curve drawn in Fig. 11 shows about 10% less anisotropy at 50° and 130° than would be predicted by $1 + \cos^2\theta$.

Features 2 and 3

A. Threshold Energies and Excitation Functions

An examination of Fig. 8 indicates that a second threshold occurs above 25 eV. The presence of a second dissociative transition is thus indicated and the associated TOF spectrum, feature 2, partially overlaps with feature 1. When the trailing edge of the TOF window is decreased to near 24 μseconds or less, contributions to the excitation function from feature 1 are eliminated. Several such excitation function showing threshold electron energies for feature 2 are presented in Fig. 13.

The first step in determining the AE from the appearance potential is to determine the mass of the detected fragment. As there is now sufficient electron energy to completely dissociate CO_2, the possibility of producing detectable carbon fragments must be considered. There are no known metastable states of carbon with sufficient internal energy to produce significant numbers of Auger electrons but presumably a carbon fragment in a high lying Rydberg state ($\sim$ 11 eV) could be detected. The minimum electron energy required for total CO_2 dissociation and production of a carbon Rydberg atom is

$$V_{min} = D_o^o(CO - O) + D_o^o(C - O) + E_c(R)$$
$$\simeq 27.6 \text{ eV}.$$

Energy considerations alone appear to eliminate a dissociative mechanism which produces Rydberg carbon atoms. If we consider a carbon atom with a TOF of 23.7 μsec or 1.78 eV kinetic energy, momentum conservation arguments show that in excess of 2.5 eV total kinetic energy is released from either a linear (asymmetric stretch) or bent (either symmetric stretch) configuration of CO_2. Therefore the threshold for producing

Rydberg carbon fragments will necessarily be in excess of 30 eV. The observed threshold is near 29 eV (Fig. 13). We note also that a C(R) atom arising from a process in which total fragmentation does not occur, namely,

$$e + CO_2 \rightarrow C(R) + O_2^*$$

cannot be excluded using an energy argument. It must be rejected, however, because of difficulties in accounting for the observed angular distribution (section B).

If, as was done for feature 1, we consider a model in which nearly all the excess electronic energy is partitioned into kinetic energy, an asymptotic energy near 25.5 eV is found, independent of kinetic energy from 2.5 eV to 3.9 eV. The vertical lines in Fig. 13 show the threshold energies calculated from Eq. 5 and assuming AE's of 25.0, 25.5 and 26.0 eV. A CO + O dissociation process was again assumed because of the following considerations: The parallel angular distribution, $I(\theta)$, for feature 2 (Section B) suggests that the excited CO_2 parent state remains linear before dissociation. Consequently, if complete fragmentation occurred, the total kinetic energy associated with a detected oxygen fragment having a TOF of 23.7 μseconds (2.4 eV) is 4.8 eV. Subtracting this from the experimental threshold of 29.2 eV gives the contradictory AE of 24.4 eV which is well below the 25.7 eV value required for total fragmentation.

In an attempt to measure the excitation function of only feature 2, the TOF window was confined to the interval from 17.6 to 20.8 μseconds (3.2 - 4.4 eV). The resulting excitation function is shown in Fig. 14 and reveals that in reality, there are two strongly overlapping TOF

spectra in this time interval. The new spectrum, feature 3, displays a threshold near 43.7 eV. This value was determined by performing least squares fits along the two linear portions of the data (see Fig. 14). The sum of the two excitation functions is seen to rise gradually, reaching a maximum near 90 eV. This implies that no electron exchange occurs in the excitation process. Other data (not shown) would suggest that the feature 2 cross section peaks near 65 eV and the maximum in Fig. 14 is for feature 3.

B. Angular Distributions

As in the case of feature 1, overlapping TOF spectra prevented an examination of $I(\theta)$ for feature 2 as a function of electron energy. Figure 15 shows $I(\theta)$ measured at 33 eV for fragments in feature 2 with TOF's between 20.5 to 23.7 μseconds (2.4 - 3.3 eV). Normalization of the data was accomplished as previously described for feature 1. The plotted curve is obtained from Eq. 3 for a parallel transition ($\Delta\Lambda = 0$) assuming θ' is 40.5 degrees. Because Eq. 3 describes $I(\theta)$ for fragments of fixed kinetic energy, the drawn curve is intended only as a qualitative fit. Dunn's[7] rules again suggest that the excited state is of Σ_u^+ symmetry and the high degree of anisotropy (Fig. 15) indicates that fragmentation occurs without significant delay.

An attempt was made to measure $I(\theta)$ for only feature 3 at 49 eV by examining particles with TOF's between 13.4 to 17 μseconds (4.7 - 7.6 eV). The angular distribution was found to be isotropic but interpretation of the data is difficult because of the number of possible explanations. An isotropic distribution could be produced by a superposition of equal contributions from features 2 (Σ_u^+) and 3(possibly π_u) or from a single transition to a bent state followed after some delay by total fragmentation.

At 49 eV, contributions from yet another feature (feature 4) may also be present.

B. Energy Distributions

While the TOF data of Fig. 6 do not readily resolve features 2 and 3, their separation is enhanced somewhat with transformations to energy spectra (Fig. 12). Feature 2 can be seen as structure between the peaks of features 1 and 3 which have maxima near 1 eV and 3.5 eV respectively. The slowest fragments of feature 2 are estimated to have TOF's near 27 μseconds (1.8 eV): feature 2 ceases to make measurable contributions to excitation functions for TOF's greater than this value.

C. Discussion

We conclude from the threshold measurements of section A that feature 2 is produced via a CO + O dissociation process, but an attempt to correlate an AE near 25.5 eV with known separated $O(^5S)$ + CO (excited) fragments was not possible (Table 1). The combination of $b^3\Sigma^+ + O^5(S^o)$ at 25 eV is not likely because the resultant parent molecule would be in a Σ^- state. Transitions between Σ^+ - Σ^- states by electron impact are strongly forbidden[25] and there would be the additional disagreement with the angular distribution result requiring an excited Σ_u^+ state.

An explanation of the feature 2 data could be provided by a mechanism in which Rydberg oxygen atoms are produced and detected. We note that the molecule - positive ion fragments of $CO(a' \ ^3\Sigma^+) + O^+$ have an AE of 25.96 eV. This would mean that combinations of $CO(a' \ ^3\Sigma^+) + O(R)$ would have AE's just below 25.96. Indeed, earlier measurements of AE's for Rydberg states have been less that the ion limit by $\sim$ 0.3 eV[1d] which would be more consistent with the present

results (near 25.5 eV). Thus the excitation of $CO_2(X^1\Sigma_g^+)$ could be to a doubly excited repulsive Rydberg state of $CO_2(^1\Sigma_u^+)$. This would explain both the shape of the excitation function as well as the angular distribution of feature 2. Spin orbit mixing would not necessarily be called for (feature 1) to explain the multiplicity of the excited $^1\Sigma_u^+$ state since the O(R) fragments could be in a triplet state.

We advance the above model as one that is plausible but acknowledge some reservations. A difficulty in attempting to analyze our results in terms of CO + O fragment combinations is that only eight of the eighteen possible electronic states of $CO[C(^3P) + O(^3P)]$ have been observed.[26] The others are thought to be weakly bound or repulsive. Some of the "missing" CO states could have energies which would make them relevant to the present problem. Potential surfaces formed by these unknown states with oxygen might provide alternative explanations to the observed data.

Feature 3 is less accessible to study by the methods of translational spectroscopy because it overlaps with features 2 and probably 4. The high threshold energy increases the likelihood of total fragmentation making any estimate of an AE suspect due to the resulting uncertainty in total kinetic energy. Lack of anisotropy in the angular distribution further obscures the analysis. Because of these reasons, no conclusions can be drawn regarding the metastable species (O or C) that is being detected or the symmetry type of the excited electronic state through which fragmentation occurs. The data in Fig. 12 do show that the most probable kinetic energy for an O fragment could be near 3.5 eV and the most energetic fragments probably exceed 5 eV.

FEATURE 4...AND 5

A. Excitation Functions and Threshold Energies

Indications for the onset of feature 4 are present in the excitation function of Feature 2 because of the wide TOF window that was used (see Fig. 13). The threshold for feature 4 is associated with the beginning of the quadratic portion of the excitation function but cannot be located well because feature 3 has similar threshold energies. By narrowing the TOF window, excitation functions were measured for what was believed to be feature 4 exclusively and several of these are presented in Fig. 16. The quadratic region is followed by a linear region which extends beyond 100 eV. Figure 16 also shows that the onset of the quadratic and linear portions are shifted to higher electron energies as more energetic fragments are examined. One possible interpretation of these data is that we are observing two transitions and further evidence for this is presented in section B. It could then follow that fragments with 6.3 eV kinetic energy are first produced from feature 4 near 39 eV and from a fifth overlapping feature near 54 eV (no correction for thermal effects has been made).

Still another interpretation is that a single excitation process is occurring and the quadratic shape of the excitation function is due to a very broad energy distribution[27] (Fig. 12). However, in this case the onset of the linear portion should not be displaced to higher electron energies when fragments of less kinetic energy are excluded from the excitation function, contrary to what does occur (Fig. 16).

B. Angular Distribution

Because there is no resolved TOF spectra faster than feature 4 (and 5), it is possible to measure $I(\theta)$ as a function of electron energy. Angular distributions for fragments with 6.3 to 9.2 eV kinetic energy are shown in Fig. 17 for two electron energies. At lower electron energies, the distributions exhibit minima near 65 and 115 degrees and maxima at 90, and possibly at 0 and 180 degrees. Measurements could not be made for angles less than ~65 degrees because of a fast overlapping TOF signal which occurred as the electron beam axis became more aligned with the detector. This feature was determined to be an artifact because of its persistence in the absence of any electron gun collector current.[28] The degree of anisotropy is reduced (as expected) when the electron energy is increased. Some asymmetry with respect to 90 degrees is present at 74 eV. A ready explanation for this is not apparent. Interactions between nearby electronic states can introduce a forward-backward asymmetry in the angular distributions.[29]

Equation 3 and 4 cannot qualitatively describe the observed distributions and one must consider theoretical distributions which include correction terms to the dipole approximation (section III). Using the results of Van Brunt[15] (his Fig. 1), it was possible to construct threshold angular distributions which, aside from greater anisotropy, resembled the present results. No quantitative fit was attempted because of the range of kinetic energies included in our data. It is significant, however, that a superposition of two transitions,

$\Sigma_g \rightarrow \pi_u(A)$ and $\Sigma_g \rightarrow \Sigma_u(A)$, is required to account qualitatively for our angular results confirming our earlier conclusion that two processes were occurring.[30] A single $\Sigma_g \rightarrow \Sigma_g$ transtion will not work. The perpendicular component (π_u) appears to lose its anisotropy more rapidly as the electron energy is increased, suggesting that it's threshold is somewhat lower than that of the Σ_u component and enabling a plausible identification of the π_u with the lower lying of the two states, i.e. feature 4.

c. Energy Distribution

As in the case of feature 3, the energy distributions for features 4 and 5 are calculated assuming that only oxygen fragments are detected (Fig. 12). Whether the fragments are oxygen or carbon, it is clear that the energy spectra are quite broad indicating that the associated potential surfaces are very steep. The strong overlapping of the spectra would suggest that the excited states have surfaces which are similar within the Franck-Condon region. We suspect that the higher lying surface (feature 5) is not quite as steep because the shift in onset electron energy as a function of kinetic energy is not as great for feature 5 (Fig. 16).

D. Discussion

Associated with studies of polyatomic molecular excitation processes having high threshold energies is a greater degree of ambiguity in interpreting the results. A scarcity of experimental as well as theoretical results in what might be regarded as one of the remaining "frontiers" in molecular physics compounds the difficulty. These observations are borne out by the discussion below.

The clear anisotropy present in the angular distribution measurements has been interpreted to mean that two states (π_u, Σ_u) have been excited and remain linear during fragmentation of the molecule. This implies

that we are detecting metastable oxygen or high lying Rydberg oxygen atoms. However, there exists the perhaps less likely possibility that the maximum at 90 degrees (feature 4) originates from a parallel transition followed by the CO_2 molecule acquiring a bent configuration. A C atom in a Rydberg state could presumably then be ejected perpendicular to the momentum transfer direction (electron beam direction at threshold) to give a maximum at 90 degrees. The total kinetic energy released would be a function of the CO_2 bending angle and normal mode. While this model would introduce a blurring of $I(\theta)$, it cannot be totally ruled out. It will be recalled that the possibility of feature 2 consisting of C fragments was rejected on the basis of threshold energy arguments. This cannot be done in the present case, although a very large bending angle would be required to explain the threshold for feature 4.

We have not been able to arrive at an unambiguous AE value for feature 4. Assuming that oxygen fragments are being detected, models of linear $OC \rightarrow O$ or $O \leftarrow C \rightarrow O$ fragmentation mechanisms do not yield a unique energy when the total kinetic energy is subtracted from the threshold energy. Similar calculations for 3 different kinetic energy fragments in feature 5 do yield a fixed energy near 42 eV if a $O \leftarrow C \rightarrow O$ dissociation process is assumed.

VI. Summary

We have examined, using the methods of translational spectroscopy and an angular distribution analysis, mechanisms for the production of metastable fragments from CO_2 following electron impact. A kinetic energy representation of the "fast feature" reveals four partially overlapping spectra. The presence of a fifth spectrum, which strongly

overlaps with feature 4, was discovered as a result of angular distribution and excitation function measurements. The approximate regions of energy space where the states leading to these spectra lie are summarized in Fig. 18.

Feature 1, the slowest of the spectra, is believed to consist of $O(^5S)$ fragments and is produced simultaneously with a metastable CO fragment through a predissociation mechanism. Excitation is initially to a Σ_u^+ state which fragments by mixing with a nearby state of π_u symmetry. Feature 2 is probably due to Rydberg oxygen fragments from a doubly excited Σ_u Rydberg state of CO_2 and dissociation occurs with no significant delay.

The metastable particles in features 3, 4 and 5 cannot be firmly identified, given the present data. The angular distributions for features 4 and 5 are most easily interpreted as arising from linear excited states of CO_2 (π_u and Σ_u) implying that oxygen fragments are being detected. This would be consistent with Freund's suggestion[1b] that Rydberg oxygen fragments are responsible for the composite fast peak. Perhaps what is most impressive about these fastest features is their large kinetic energy.

Acknowledgement

We are pleased to acknowledge useful discussions with Dr. Richard Van Brunt during his summer stay at Goddard Space Flight Center.

References

1.(a) R.S. Freund and W. Klemperer, J. Chem. Phys. 47, 2897 (1967).

(b) R.S. Freund, J. Chem. Phys. 55, 3569 (1971).

(c) R.S. Freund, J. Chem. Phys. 54, 3125 (1971).

(d) K.C. Smyth, J.A. Schiavone and R.S. Freund, J. Chem. Phys. 59, 5225 (1973).

2. M. Misakian and J.C. Zorn, Phys. Rev. A. 6, 2180 (1972).

3.(a) G.E. Busch and K.R. Wilson, J. Chem. Phys. 56, 3626 (1972).

(b) G.E. Busch and K.R. Wilson, J. Chem. Phys. 56, 3655 (1972).

4.(a) W.C. Wells, W.L. Borst and E.C. Zipf, J. Geophys. Res. 74, 6515 (1969)

(b) W.L. Borst and E.C. Zipf, Phys. Rev. A 4, 153 (1971).

(c) W.C. Wells, W.L. Borst and E.C. Zipf, J. Geophys. Res. 77, 69 (1972).

5. M. Levanthal, R.T. Robiscoe, and K.R. Lea, Phys. Rev. 158, 49 (1969).
R. Clampitt and A.S. Newton, J. Chem. Phys. 50, 1997 (1969).

6. Throughout the remainder of this article, the use of the expression "asymptotic energy" for a fragmentation process will be taken to mean the potential energy of separated O - CO fragments where the CO molecule is in its lowest vibrational level.

7. G.H. Dunn, Phys. Rev. Letters 8, 62 (1962).

8. See G. Herzberg, Molecular Spectra and Molecular Structure, Vol. III, (Van Nostrand Reinhold, New York, 1966) for a comprehensive treatment of dissociation processes in polyatomic molecules.

9. K. Holdy, L.C. Klotz and K.R. Wilson, J. Chem. Phys. 52, 4588 (1970).

10. P.J. Chantry and G.J. Schulz, Phys. Rev. 156, 134 (1967).

11. The electronic eigenfunctions given by Σ_u^+, π_g, etc. are solutions of the CO_2 Hamiltonian describing the molecule with all three nuclei fixed in space. When the interaction of the electronic and nuclear motions are considered, it is found that the rotational and vibrational motions of the nuclei act as perturbations which can mix nearby electronic states of the same total angular momentum J, parity (+ or -), symmetry (g g, u u, g u), and spin S. Electronic states which interact because of vibrational motion (homogeneous perturbation) are characterized by $\Delta\Lambda = 0$ and for the case of rotational motion (heterogeneous perturbation), $\Delta\Lambda = \pm 1$; see ref. 8 for a full discussion.

12. R.N. Zare and D.R. Herschbach, Proc. IEEE 51, 173 (1963).

13. R.N. Zare, Ph.D. Thesis, Harvard University, 1964 (unpublished).

14. G.H. Dunn and L.J. Kieffer, Phys. Rev. 132, 2109 (1963).
R.J. Van Brunt and L.J. Kieffer, Phys. Rev. A2, 1293 (1970).
M. Misakian, J.C. Pearl and M.J. Mumma, J. Chem. Phys. 57, 1891 (1972).

15. R.J. Van Brunt, J. Chem. Phys. 60, 3064 (1974).

16. R.J. Van Brunt and L.J. Kieffer, J. Chem. Phys. 60, 3057 (1974).
R.J. Van Brunt and L.J. Kieffer, Phys. Rev A, in press.
R.J. Van Brunt, G.M. Lawrence, L.J. Kieffer and J.M. Slater, J. Chem. Phys., in press.

17. C. Jonah, J. Chem. Phys. 55, 1915 (1971).

18. M. Misakian and M.J. Mumma, Rev. Sci. Instrum. 45, 296 (1974).

19. M.J. Mumma and E.C. Zipf, J. Chem. Phys. 55, 1661 (1971).

20. M.J. Mumma, M. Misakian, W.M. Jackson and J.L. Faris, Phys. Rev. A 9, 203 (1974).

21. J.C. Pearl, Ph.D. dissertation, University of Michigan, 1970 (unpublished). See Ref. 2 also.

22. The photon TOF from helium gas showed a sharp cut off indicating that the electron gun current was indeed following the on-off pulse shape.

23. Such a mechanism has previously been invoked (M. Krauss, S.R. Mielczarek, D. Neumann and C.E. Kuyatt, J. Geophys. Res. 76, 3733 (1971)) to explain a violation of the selection rule $\Delta S = 0$ in CO_2.

24. The ground configuration of CO_2 may be written

$$CO_2(X^1\Sigma_g^+)(1\sigma_g)^2(1\sigma_u)^2(2\sigma_g)^2(3\sigma_g)^2(2\sigma_u)^2$$
$$(4\sigma_g)^2(3\sigma_u)^2(1\pi_u)^4(1\pi_g)^4.$$

The outer shell electrons have vertical ionization potentials of 13.8, 17.6, 18.1 and 19.4 eV, corresponding to removal of a single electron from the $1\pi_g$, $1\pi_u$, $3\sigma_u$ and $4\sigma_g$ orbitals respectively (C.R. Brundle and D.W. Turner, Intern. J. Mass Spectrometry Ion Phys. 2, 195 (1969)). The next least tightly bound orbital, $2\sigma_u$, requires about 40 eV for ionization and its Rydbergs lie within (nominally) 4 eV of the ionization limit. Thus, there can be no singly excited states between 20 and $\sim$ 36 eV. Similar problems are encountered for production of photons from CO_2 by electron impact (see M.J. Mumma, E.J. Stone, W.L. Borst and E.C. Zipf, J. Chem. Phys. 57, 68 (1972)).

25. D.C. Cartwright, S. Trajmar, W. Williams and D.L. Huestis, Phys. Rev. Letters 27, 704 (1971).

26. P.H. Krupenie, Natl. Std. Ref. Data Ser., Natl. Bur. Std. (U.S.) 5 (1966).

27. A similar behavior has been observed by A. Crowe and J.W. McConkey (J. Phys. B 7, 349 (1974)) for the production of O^+ and C^+ from the dissociative ionization of CO_2. It is interesting to further note that the excitation processes they observe appear to be characterized in large part, as in the present study, by parallel transitions.

28. By "floating" the electron gun cathode and pulsing the Pierce element, it was possible to generate a very fast TOF at small angles without collector currents.

29. T.F. O'Malley and H.S. Taylor, Phys. Rev. 176, 207 (1968). R.J. Van Brunt and L.J. Kieffer, Phys. Rev. A 2, 1899 (1970).

30. See Ref. 15 for explanation of $\Sigma_u(A)$ and $\pi_u(A)$ notation.

Figure Captions

Fig. 1 (a) A schematic description of the CO_2 dissociation process is shown. The two bending modes are suppressed. The trajectory shown is for direct and immediate fragmentation. The released kinetic energy will be a function of the CO fragment internal energy.

(b) Cross sections of several surfaces which can interact during a predissociation process.

Fig. 2. Behavior of transition matrix element between pairs of electronic states with electron energies at threshold (after Ref. 7). Entries to the left of the vertical bars indicate matrix element behavior for perpendicular molecular orientations and entries to the right are for parallel orientations. Qualitative angular distributions of the fragment are also shown assuming dissociation occurs in a time which is short compared to the period of rotation.

Fig. 3. Schematic view of electron gun and detector. The electron gun could be rotated about an axis perpendicular to the center of the collision chamber. Ions and scattered electrons were removed from the beam with deflection plates in the slit system.

Fig. 4. Schematic of TOF electronics.

Fig. 5. Full TOF spectrum of metastable fragments from CO_2 showing the slow and fast peaks. The dwell time was 320 nsec/channel.

Fig. 6. TOF spectra as a function of electron energy. The electron gun pulse width and path length were 1 μsec and 12.8 cm respectively. A dwell time of 320 nsec per channel was used.

Fig. 7. Normalized TOF spectra as a function of electron energy. The photons are not shown.

Fig. 8. Threshold measurements for the production of fragments in feature 1 as a function of TOF window. Calculated threshold energies assuming an AE of 20.5 eV are indicated. The enclosing vertical bars show the range for threshold energies if the AE is varied from 20.0 to 21.0 eV.

Fig. 9. Relation of parameters in Eq. 5.

Fig. 10. Excitation function for feature 1.

Fig. 11. Angular distribution of metastable O fragments in feature 1 with 0.8 to 1.5 eV kinetic energy in feature 1. The minimum at 90° is characteristic of a parallel transition. The large isotropic component suggests a predissociation mechanism. The dashed curve is drawn to fit the data.

Fig. 12. Kinetic energy distributions as a function of electron energy. The approximate locations of features 1 → 5 are indicated. The transformation from TOF to energy spectra has been made assuming only oxygen fragments are being detected. No correction has been made for the thermal motion of the parent molecules or for the small distortion produced by the 0.8 μsec pulse width.

Fig. 13. Threshold measurements for the production of fragments in feature 2 for various TOF windows. Calculated threshold

energies assuming an AE of 25.5 eV are indicated. The enclosing vertical bars show the range of threshold energies if the AE is varied from 25 to 26 eV.

Fig. 14. Excitation function for features 2 and 3. The shallow bend near 43 eV indicates the onset for feature 3.

Fig. 15. Angular distribution of oxygen fragments with 2.4 to 3.3 eV kinetic energy in feature 2. The high degree of anisotropy suggests immediate dissociation for this parallel transition. The curve has been obtained from Eq. 3 assuming θ' is 40.5 degrees.

Fig. 16. Excitation function and threshold energies for features 4 and 5. Both onset energies are observed to shift as a function of fragment kinetic energy.

Fig. 17. Angular distribution of features 4 and 5. A superposition of two transitions is necessary to explain the data.

Fig. 18. Approximate location in energy space of the states leading to the five time-of-flight features. The present data do not permit an accurate determination of the bounds on the energy ranges for features 3, 4 and 5. Only the lower bound of feature 2 can be estimated. The fourth, fifth, and sixth ionization limits of CO_2 are shown and demonstrate that features 1, 2, 4, and 5 cannot be produced by single-electron excitation. The asymptotic energies (AE's) for features 1 and 2 are also shown.

TABLE I

ASYMPTOTIC ENERGIES (eV) OF CO_2 FOR VARIOUS STATES OF CO + O FRAGMENTS

CO		OXYGEN					
		^3P	^1D	^1S	$^5S^o$	^5P	^3S
$X\,^1\Sigma^+$	0.0	5.5	7.5	9.7	14.6	15.7	15.0
$a\,^3\pi$	6.0	11.5	13.5	15.7	20.6	21.7	21.0
$a'\,^3\Sigma^+$	6.9	12.4	14.4	16.6	21.5	22.6	21.9
$d\,^3\Delta$	7.5	13.0	15.0	17.2	22.1	23.2	22.5
$e\,^3\Sigma^-$	7.9	13.4	15.4	17.6	22.5	23.6	22.9
$b\,^3\Sigma^+$	10.4	15.9	17.9	20.1	25.0	26.1	25.4

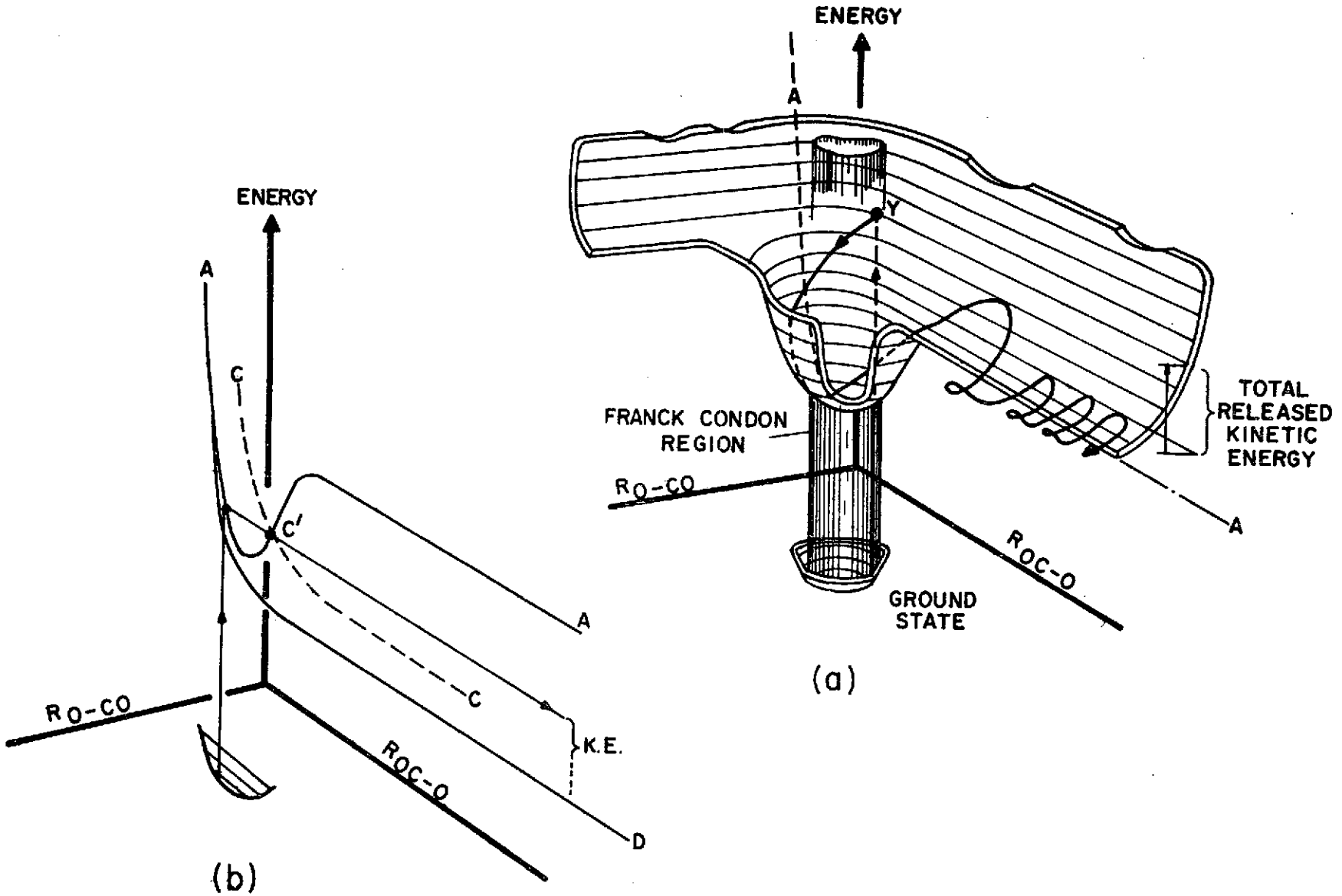
ENERGY
A
Y
FRANCK CONDON
REGION
TOTAL
RELEASED
KINETIC
ENERGY
RO-CO
A
ROC-O
GROUND
STATE
(a)
ENERGY
A
C
C'
A
C
K.E.
RO-CO
ROC-O
D
(b)

	Σ_g^+	Σ_g^-	Σ_u^+	Σ_u^-	Π_g	Π_u	Δ_g	Δ_u	(FINAL STATE)
(GROUND STATE) Σ_g^+	X | X	O | O	O | X	O | O	O | O	X | O	X | O	O | O	

MOLECULAR AXIS ⊥ TO SYMMETRY AXIS | MOLECULAR AXIS ∥ TO SYMMETRY AXIS

O..... m.e.=0

X..... m.e.≠0

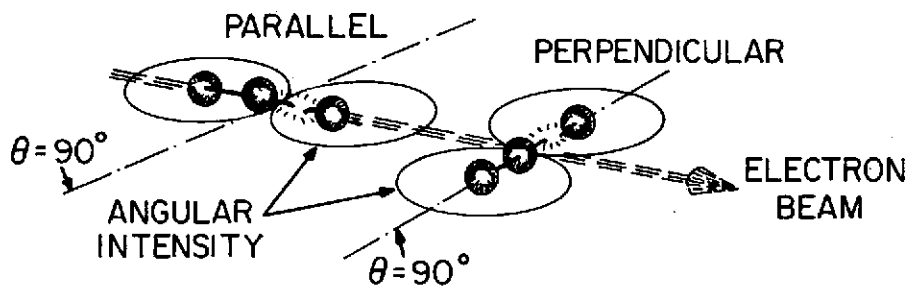

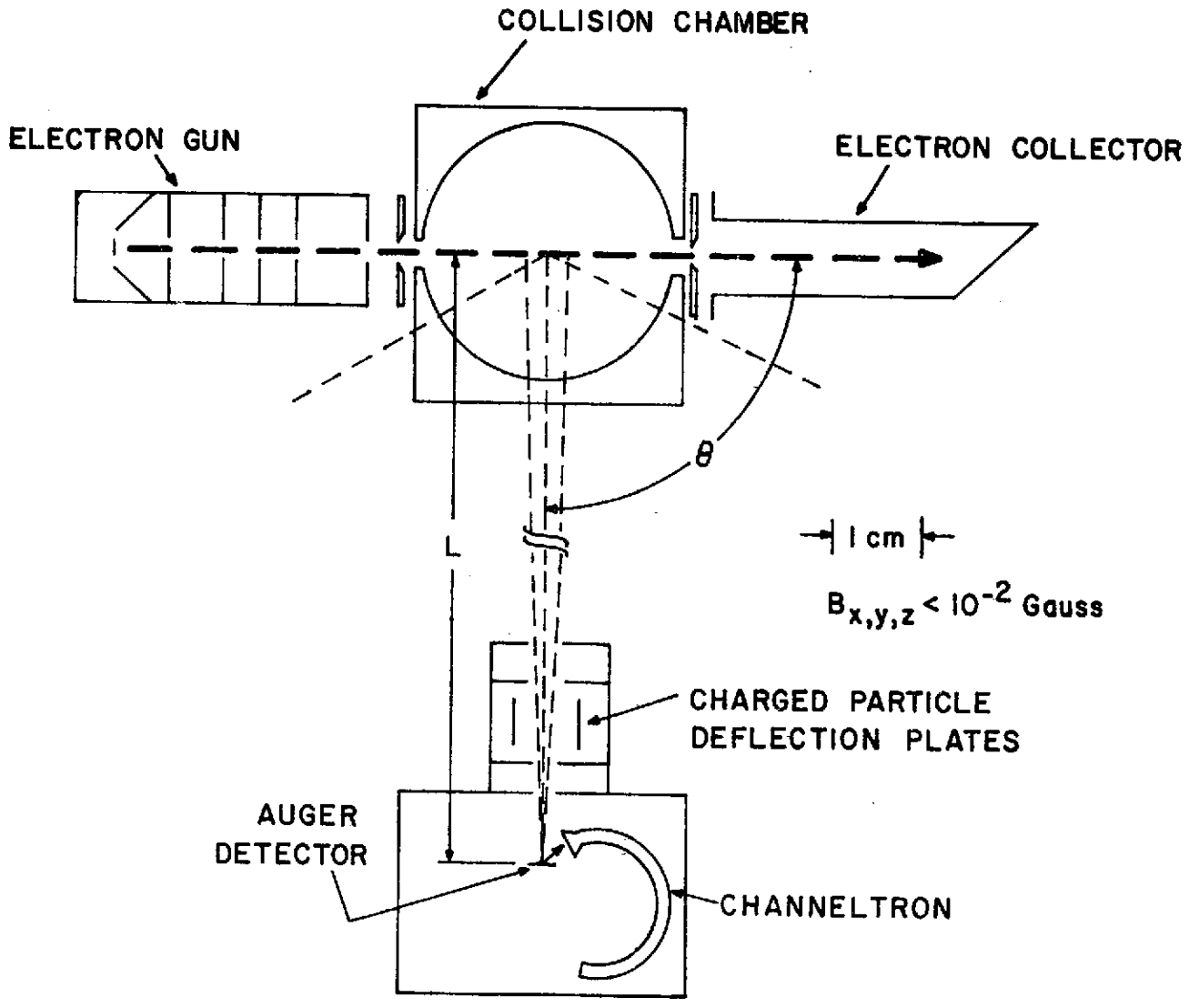
COLLISION CHAMBER
ELECTRON GUN
ELECTRON COLLECTOR
θ
L
1 cm
$B_{x,y,z} < 10^{-2}$ Gauss
CHARGED PARTICLE
DEFLECTION PLATES
AUGER
DETECTOR
CHANNELTRON

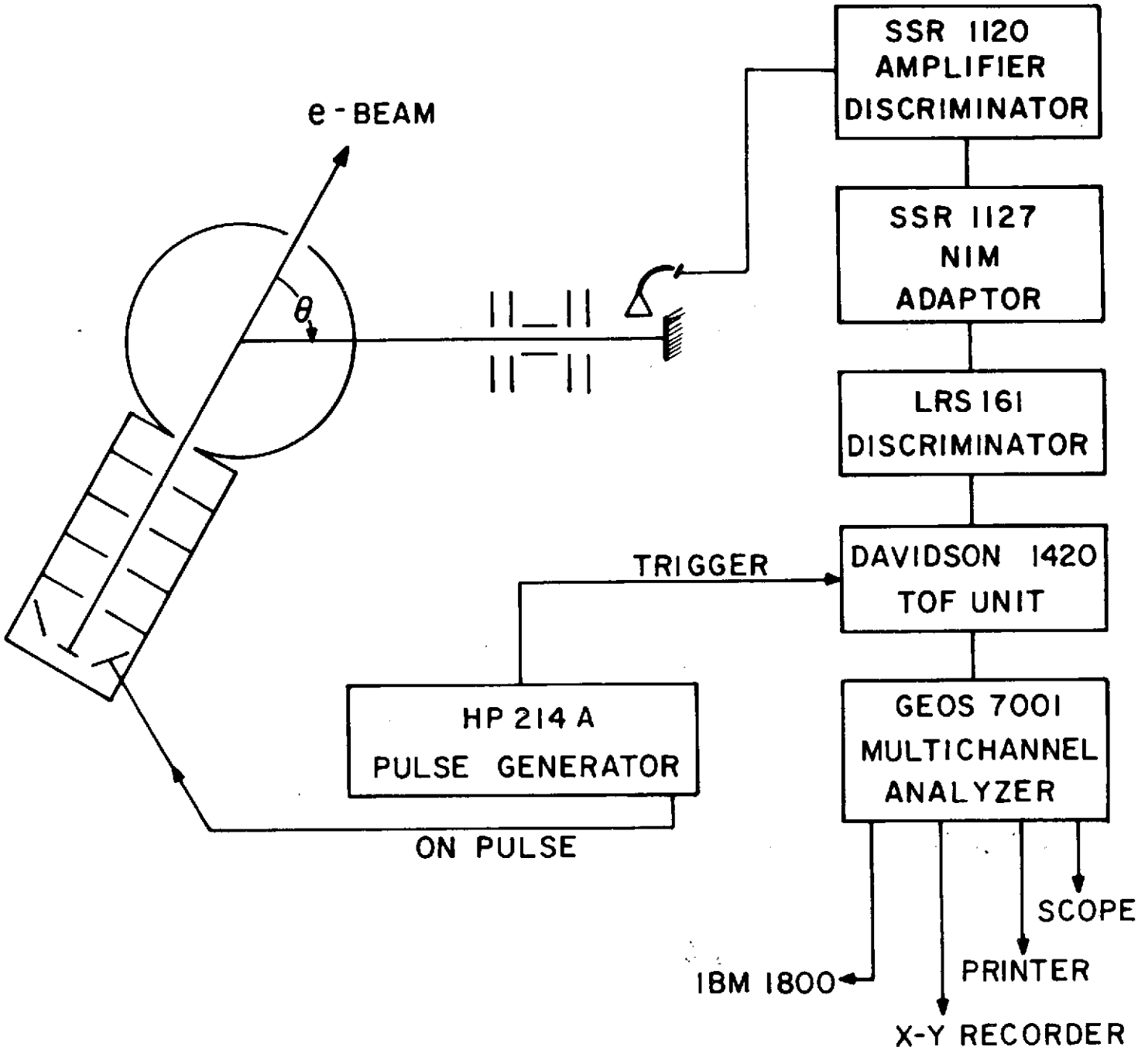
SSR 1120
AMPLIFIER
DISCRIMINATOR
e - BEAM
SSR 1127
NIM
ADAPTOR
θ
LRS 161
DISCRIMINATOR
TRIGGER
DAVIDSON 1420
TOF UNIT
HP 214 A
PULSE GENERATOR
GEOS 7001
MULTICHANNEL
ANALYZER
ON PULSE
SCOPE
IBM 1800
PRINTER
X-Y RECORDER

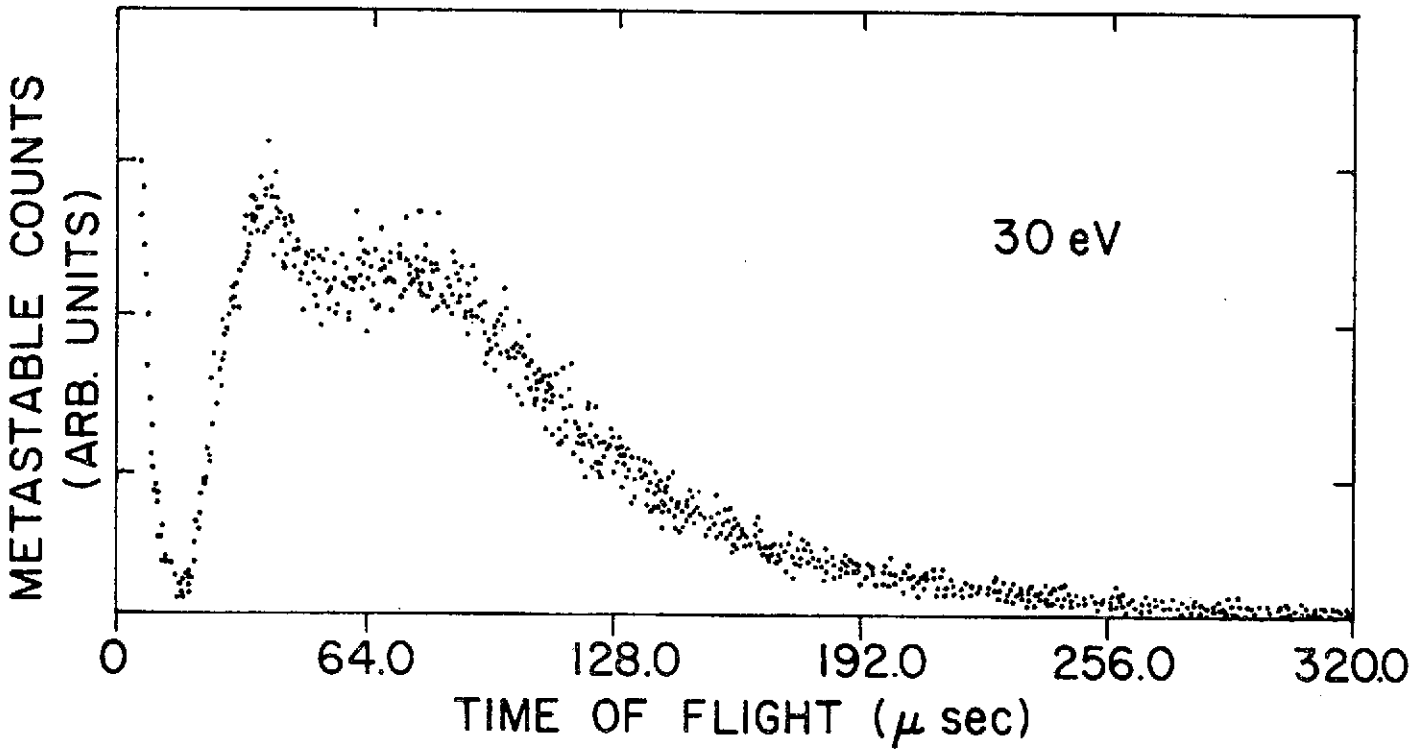
METASTABLE COUNTS
(ARB. UNITS)
30 eV
0
64.0
128.0
192.0
256.0
320.0
TIME OF FLIGHT (μ sec)

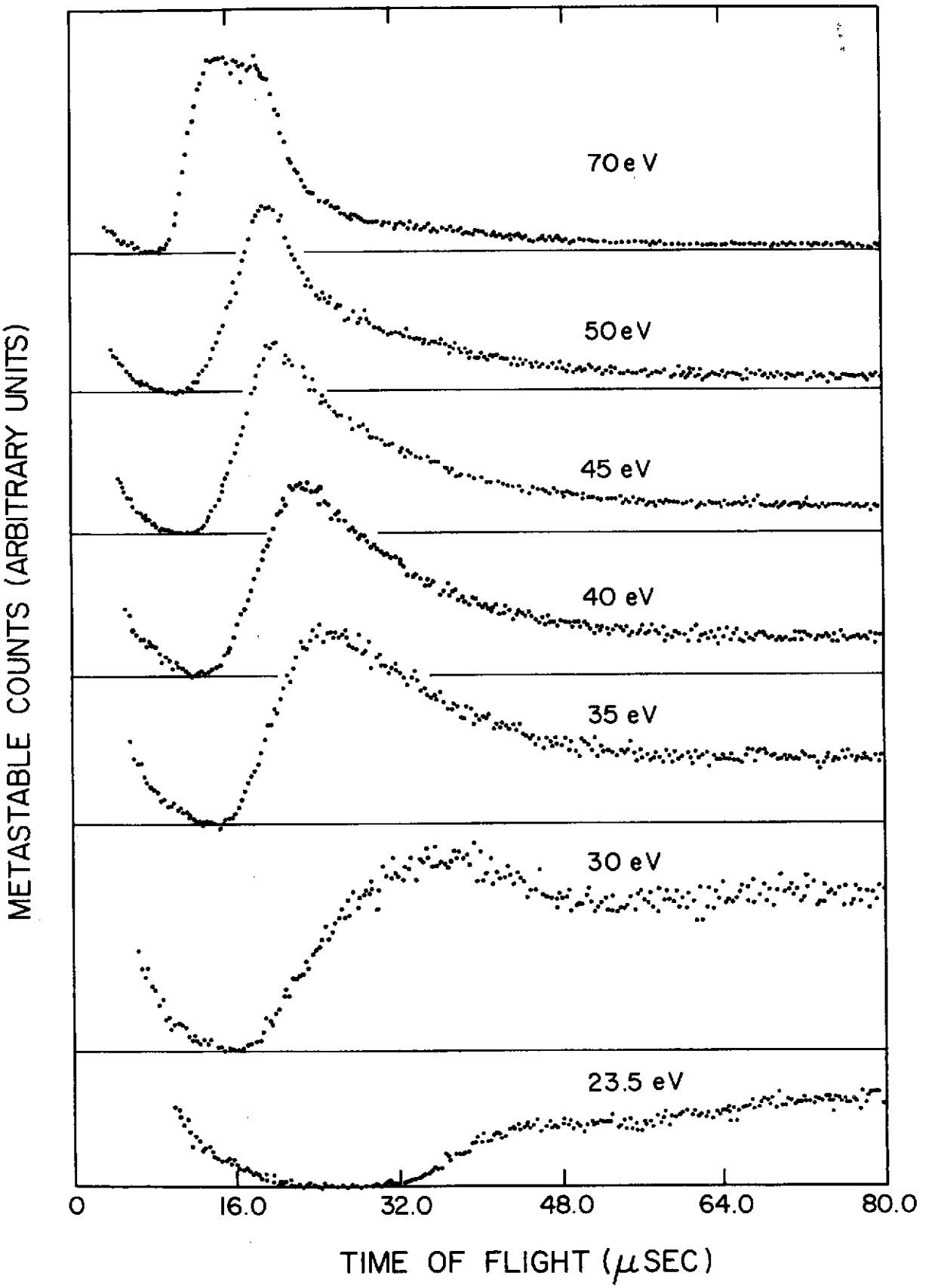
70 eV
50 eV
45 eV
40 eV
35 eV
30 eV
23.5 eV
METASTABLE COUNTS (ARBITRARY UNITS)
0
16.0
32.0
48.0
64.0
80.0
TIME OF FLIGHT (μSEC)

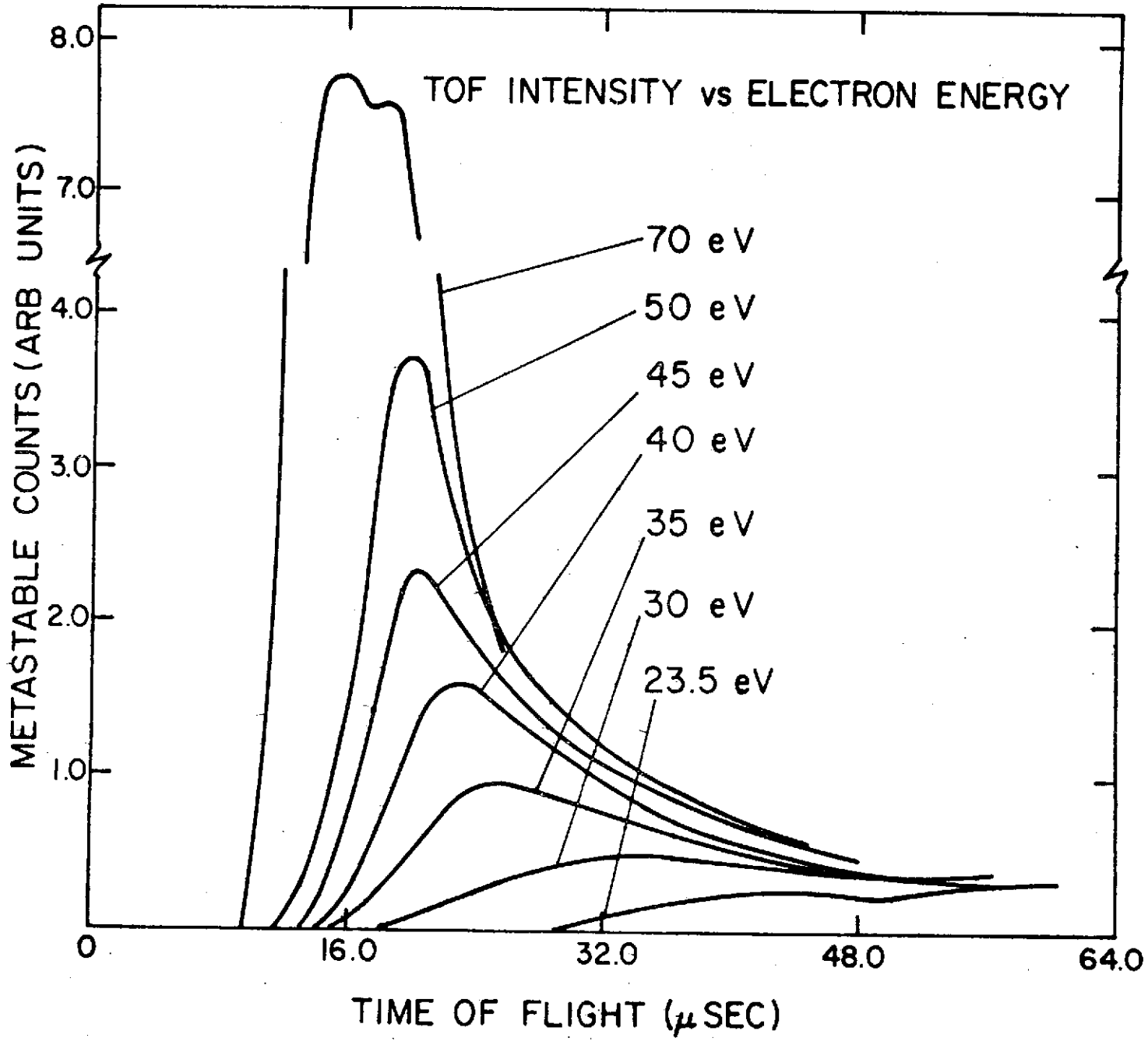
TOF INTENSITY vs ELECTRON ENERGY
METASTABLE COUNTS (ARB UNITS)
8.0
7.0
4.0
3.0
2.0
1.0
0
16.0
32.0
48.0
64.0
TIME OF FLIGHT (μSEC)
70 eV
50 eV
45 eV
40 eV
35 eV
30 eV
23.5 eV

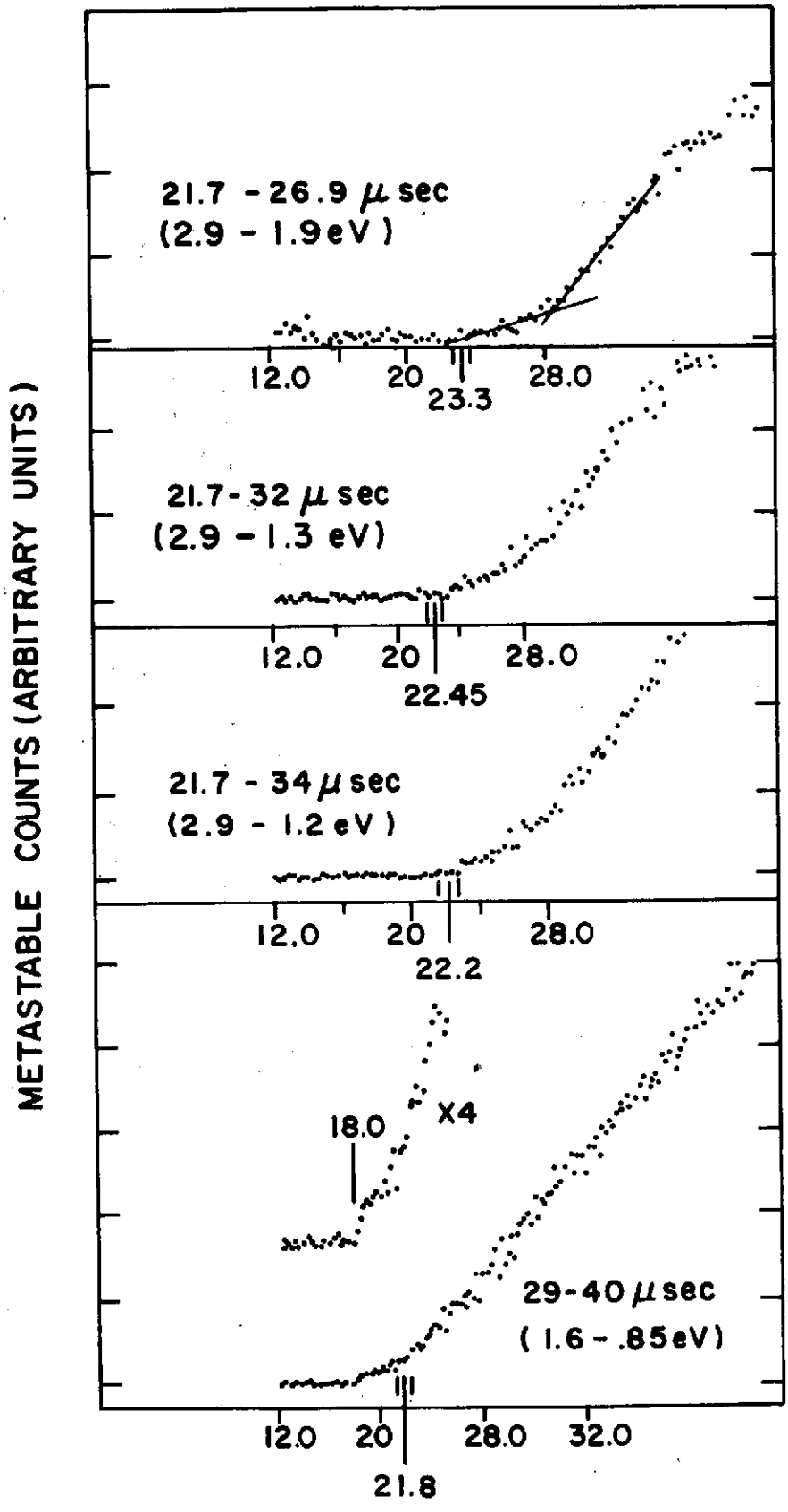
21.7 - 26.9 μ sec
(2.9 - 1.9 eV)
12.0
20
23.3
28.0
21.7 - 32 μ sec
(2.9 - 1.3 eV)
12.0
20
22.45
28.0
21.7 - 34 μ sec
(2.9 - 1.2 eV)
12.0
20
22.2
28.0
18.0
X4
29-40 μ sec
(1.6 - .85 eV)
12.0
20
21.8
28.0
32.0
METASTABLE COUNTS (ARBITRARY UNITS)
ELECTRON ENERGY (eV)

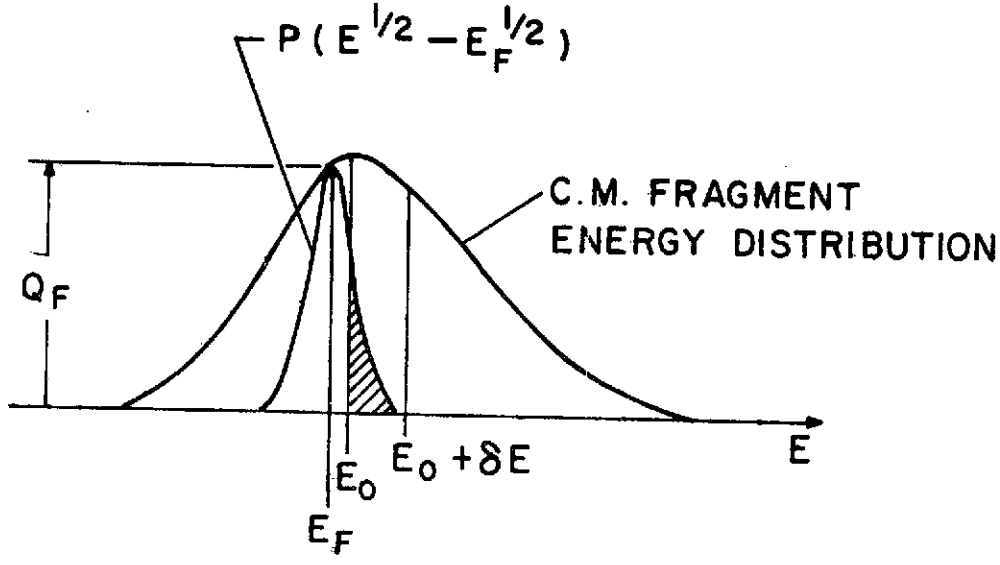
P (E 1/2 − E F 1/2)
C.M. FRAGMENT
ENERGY DISTRIBUTION
Q F
E 0
E 0 + δE
E
E F

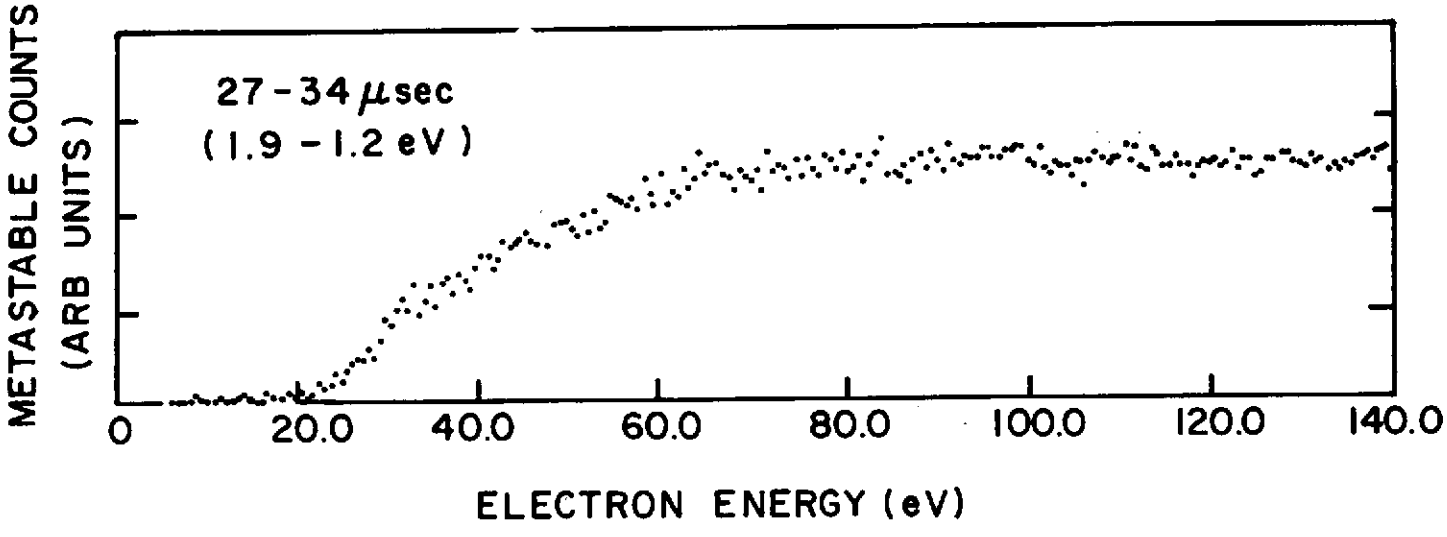
METASTABLE COUNTS
(ARB UNITS)
27 - 34 μsec
(1.9 - 1.2 eV)
0
20.0
40.0
60.0
80.0
100.0
120.0
140.0
ELECTRON ENERGY (eV)

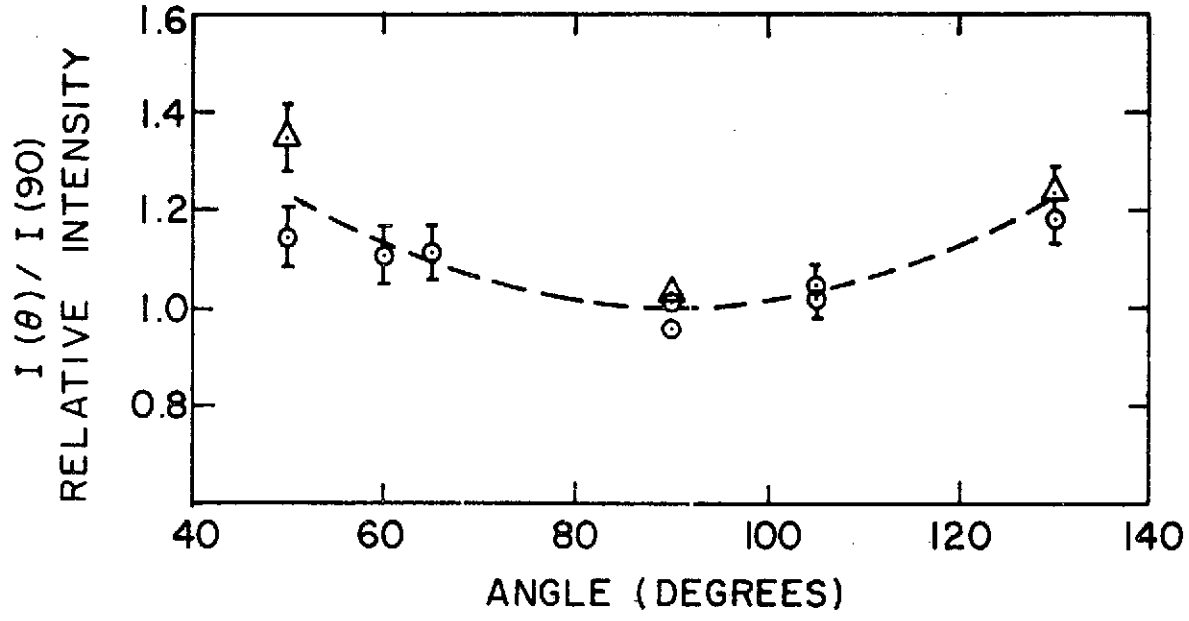
1.6
1.4
1.2
1.0
0.8
I (θ) / I (90)
RELATIVE INTENSITY
40
60
80
100
120
140
ANGLE (DEGREES)

5th

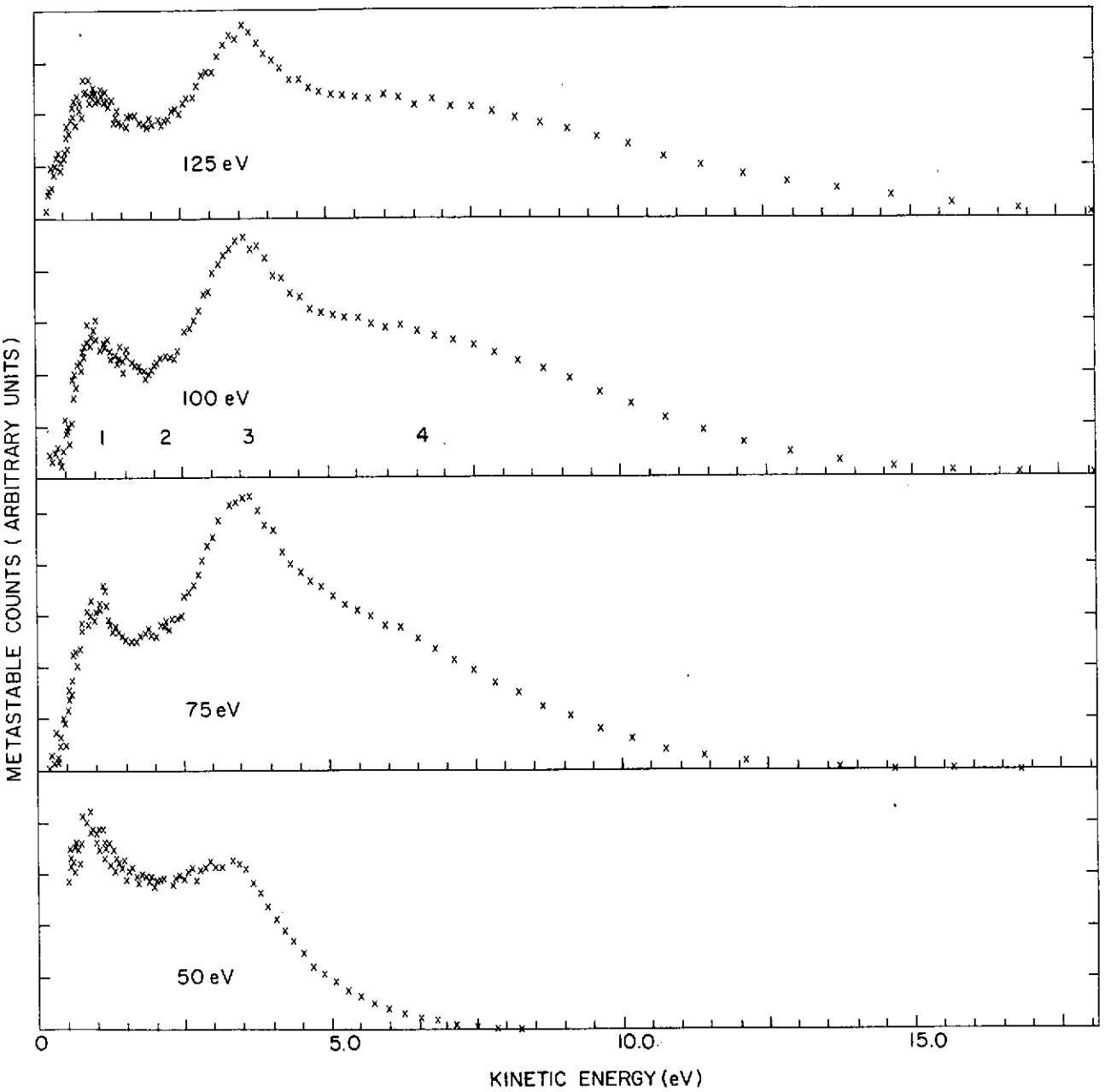
125 eV
100 eV
1
2
3
4
75 eV
50 eV
METASTABLE COUNTS (ARBITRARY UNITS)
0
5.0
10.0
15.0
KINETIC ENERGY (eV)

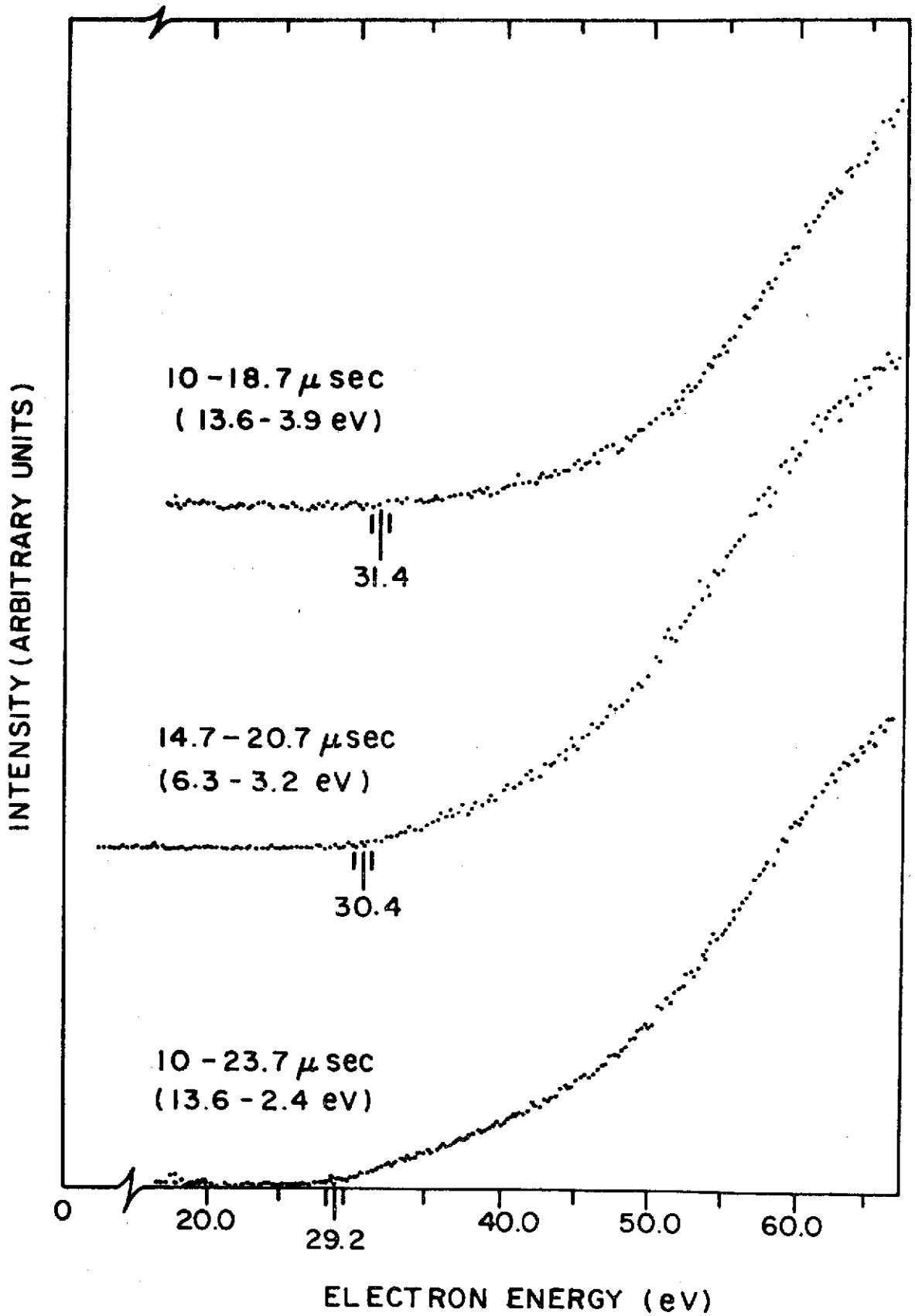
10 - 18.7 μ sec
(13.6 - 3.9 eV)
31.4
14.7 - 20.7 μ sec
(6.3 - 3.2 eV)
30.4
10 - 23.7 μ sec
(13.6 - 2.4 eV)
INTENSITY (ARBITRARY UNITS)
0
20.0
29.2
40.0
50.0
60.0
ELECTRON ENERGY (eV)

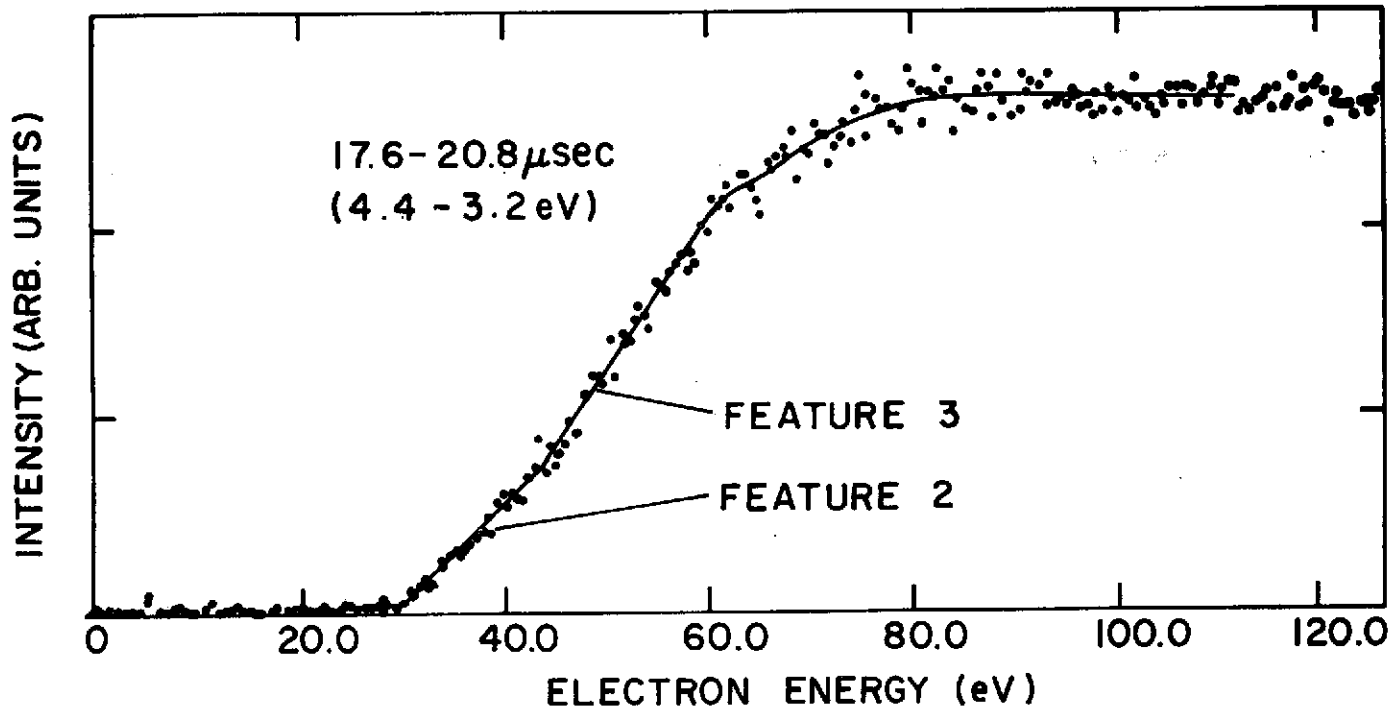
17.6-20.8μsec
(4.4 - 3.2 eV)
FEATURE 3
FEATURE 2
INTENSITY (ARB. UNITS)
0
20.0
40.0
60.0
80.0
100.0
120.0
ELECTRON ENERGY (eV)

87

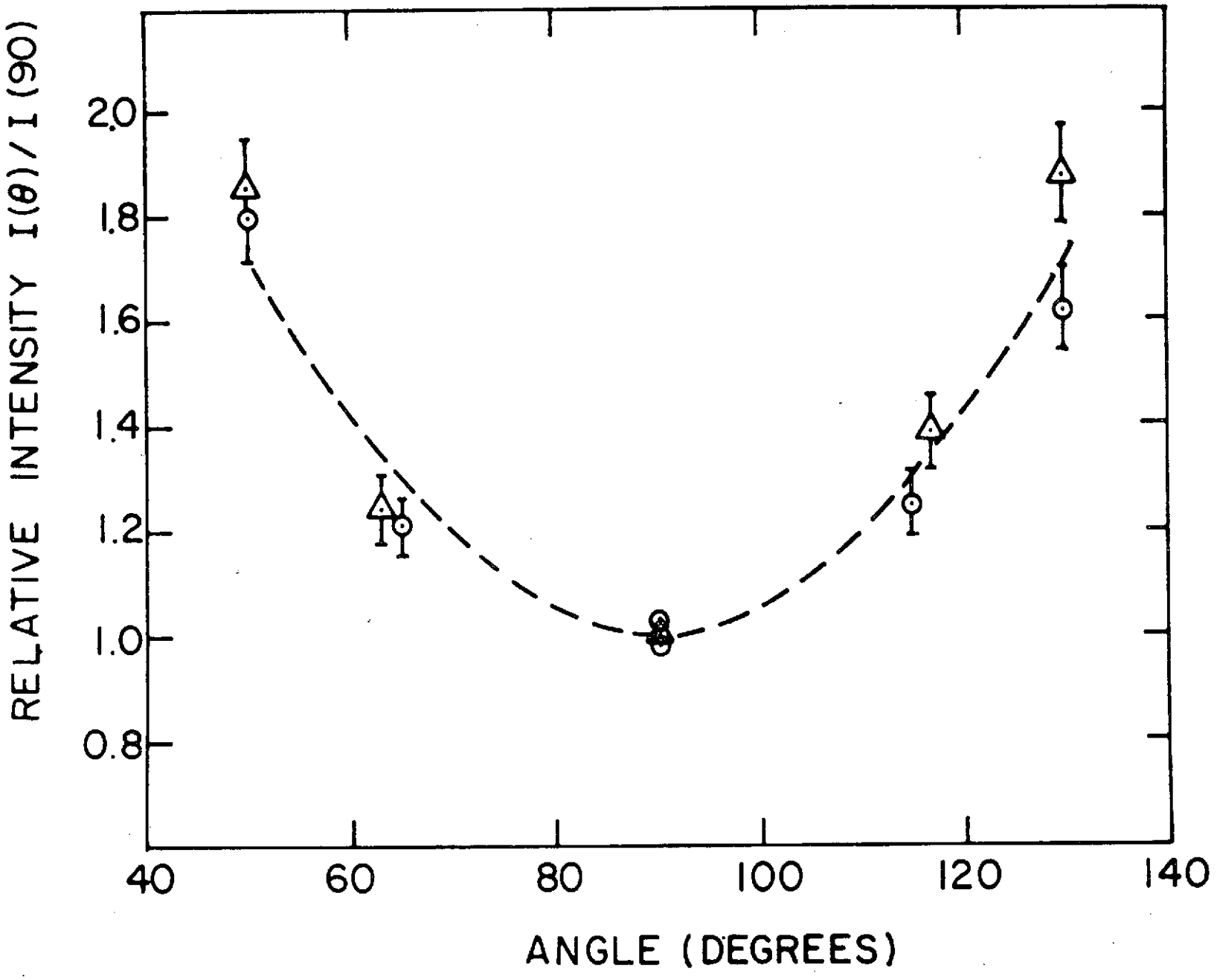
RELATIVE INTENSITY I(θ)/I(90)
2.0
1.8
1.6
1.4
1.2
1.0
0.8
40
60
80
100
120
140
ANGLE (DEGREES)

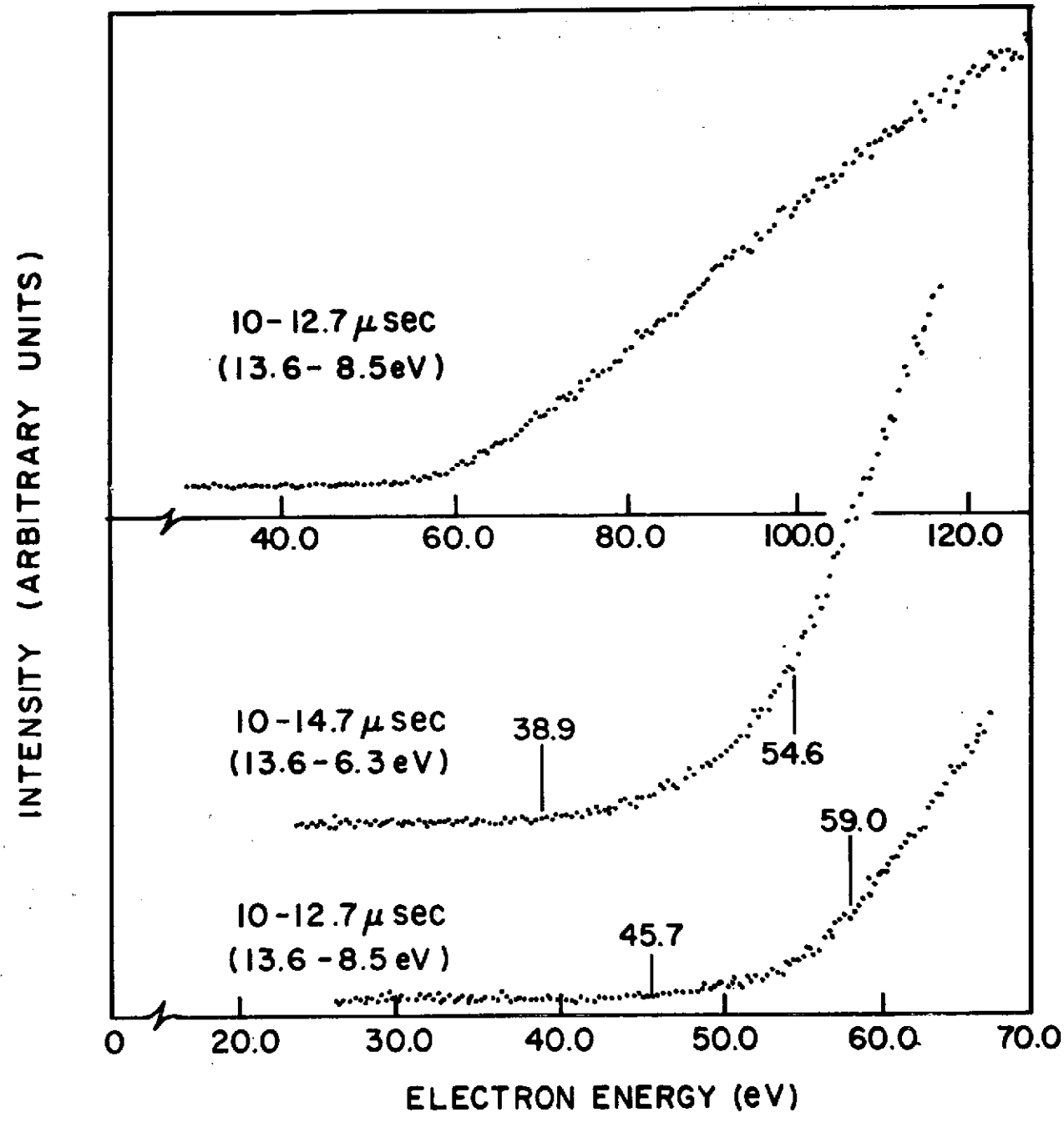
INTENSITY (ARBITRARY UNITS)
10-12.7 μsec
(13.6-8.5eV)
40.0
60.0
80.0
100.0
120.0
10-14.7 μsec
(13.6-6.3 eV)
38.9
54.6
59.0
10-12.7 μsec
(13.6-8.5 eV)
45.7
0
20.0
30.0
40.0
50.0
60.0
70.0
ELECTRON ENERGY (eV)

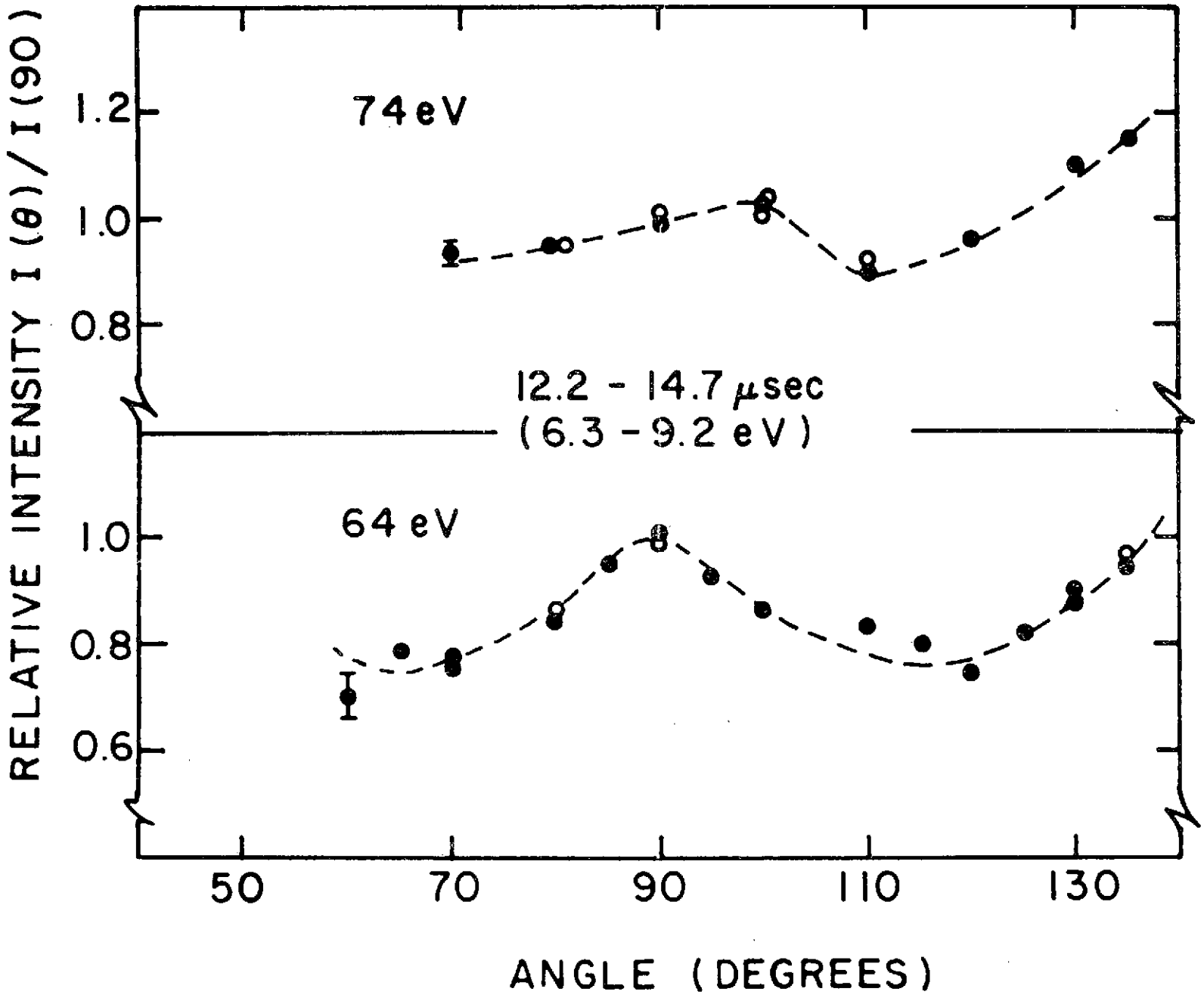
RELATIVE INTENSITY I(θ)/I(90)
74 eV
1.2
1.0
0.8
12.2 - 14.7 μsec
(6.3 - 9.2 eV)
64 eV
1.0
0.8
0.6
50
70
90
110
130
ANGLE (DEGREES)

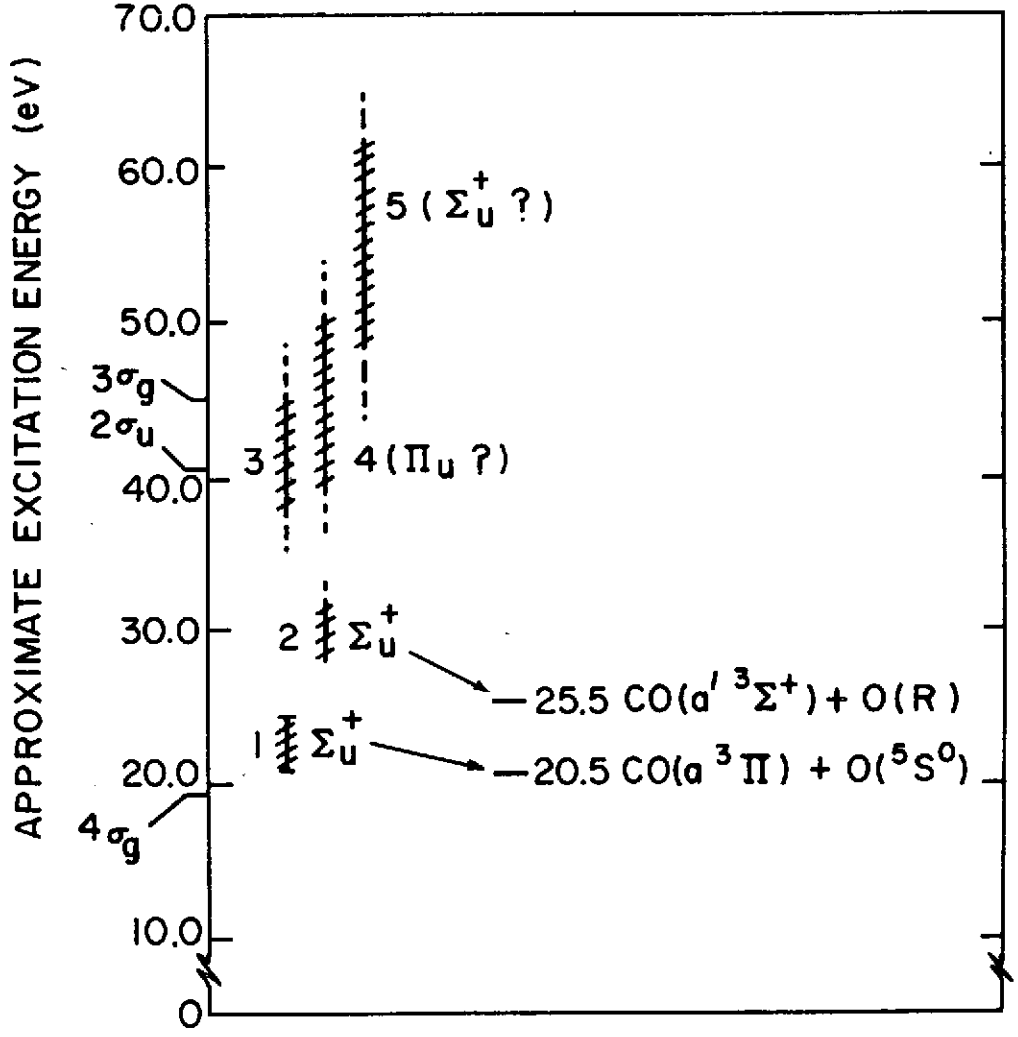
APPROXIMATE EXCITATION ENERGY (eV)
70.0
60.0
50.0
40.0
30.0
20.0
10.0
0
$3\sigma_g$
$2\sigma_u$
$4\sigma_g$
5 (Σ_u^+ ?)
4 (Π_u ?)
3
2 Σ_u^+
1 Σ_u^+
— 25.5 CO($a'\,^3\Sigma^+$) + O(R)
— 20.5 CO($a\,^3\Pi$) + O($^5S^0$)